https://ntrs.nasa.gov/search.jsp?R=19930087809 2020-06-17T12:23:53+00:00Z

N62 61989

NACA RM E53D08

CASE FILE COPY

RESEARCH MEMORANDUM

PRELIMINARY EXPERIMENTAL INVESTIGATION OF TRANSPIRATION COOLING FOR AN AFTERBURNER WITH A SINTERED, POROUS STAINLESS-STEEL COMBUSTION-CHAMBER WALL

By William K. Koffel

Lewis Flight Propulsion Laboratory
Cleveland, Ohio

NATIONAL ADVISORY COMMITTEE FOR AERONAUTICS

WASHINGTON

June 8, 1953
Declassified April 5, 1958

NATIONAL ADVISORY COMMITTEE FOR AERONAUTICS

RESEARCH MEMORANDUM

PRELIMINARY EXPERIMENTAL INVESTIGATION OF TRANSPIRATION COOLING FOR AN AFTERBURNER WITH A SINTERED, POROUS STAINLESS-STEEL COMBUSTION-CHAMBER WALL

By William K. Koffel

2833

CF-1

SUMMARY

The application of transpiration air-cooling to the combustion-chamber wall of an afterburner was investigated experimentally. The combustion-chamber wall of a full-scale afterburner was fabricated from commercially available, sintered, porous stainless-steel plate. The temperatures of the hot-gas surface of the porous wall at three stations along the wall were correlated, in terms of the local temperatures of the combustion gas and cooling air against the ratio of the cooling-air flux density normal to the porous wall to the combustion-gas flow per unit of combustion-chamber flow area. The correlation obtained from this afterburner is in good agreement with similar experimental correlations obtained for an air-cooled, sintered, porous turbine blade of stainless steel and for a nitrogen-cooled, porous section of a rocket combustion chamber.

In this investigation, oxidation of the porous metal, attributed to nonuniformities in the permeability and thickness of the porous wall became a problem wherever the wall temperature exceeded about 1600° R. The problem of oxidation can no doubt be eliminated by better design practice and improved fabrication techniques of more nearly uniform porous materials. However, the comparisons of cooling-air requirements for transpiration cooling and for forced-convection cooling in this report were made at the average limiting temperatures of 1560° R for the porous wall and 1760° R for the solid wall.

Calculations based on the experimental correlation of this investigation indicated that for an exhaust-gas total temperature of 3798° R, a burner-inlet total temperature of 1656° R, an inlet cooling-air temperature of 533° R, and a combustion-gas flow of 0.057 pound per second per square inch of burner flow area at the flame holder, a constant wall temperature of 1560° R can be maintained by transpiration cooling for a coolant-flow ratio of 0.016. This coolant-flow ratio is only 8 to 11 percent of that required to maintain an average maximum wall temperature of 1760° R under similar operating conditions for a solid-wall

forced convection cooled by air flowing through a 1/2-inch annular cooling shroud. Calculations also indicate that the transpiration cooling requirements are more than doubled for this afterburner, if, rather than maintaining a uniform wall temperature, the walls are fabricated from a uniform-permeability metal so that the maximum wall temperature is 1560° R.

INTRODUCTION

2833

Because of the military demand for ever-increasing thrust augmentation of turbojet power plants by afterburning, the engine and airframe designers must supply large quantities of air for cooling purposes. For example, experimental afterburners cooled by the parallel flow of air through an annular passage surrounding the combustion chamber require coolant-flow ratios (cooling air to combustion gas) of about 0.15 to 0.22 to maintain an average wall temperature of 1760° R at the exhaust-nozzle inlet for exhaust-gas temperatures of 3800° R (refs. 1 and 2). Practical considerations of the source and quantity of cooling air to be handled, space for ducting, pressure losses, pumping problems, and weight, each affecting the over-all power-plant performance, however, limit the maximum cooling-air flows to about 0.05 to 0.10 of the combustion-gas flow. These limitations on cooling-air flow for systems using forced-convective cooling restrict the maximum combustion-gas temperature in the afterburner and, consequently, limit the maximum thrust. Further development is required for adequate forced-convective cooling of afterburners operating at gas temperatures of 3800° to 4000° R with coolant-flow ratios of 0.05 to 0.10. For example, the development of thick ceramic coatings which would limit the flow of heat to the afterburner wall might be a possible process.

A search for more effective ways of utilizing the cooling air in turbojet afterburners led to the consideration of transpiration cooling. Experimental investigations of gaseous transpiration cooling show very effective cooling of a rocket (ref. 3) and of a gas-turbine blade (ref. 4). The application of transpiration cooling to the combustion-chamber walls of turbojet afterburners is being investigated at the NACA Lewis laboratory, and the preliminary experimental investigation of an afterburner with a sintered porous wall is reported herein.

The mechanism of transpiration cooling and a discussion of some problems in applying this method of cooling to gas-turbine blades are presented in reference 5. The theoretical heat-transfer processes were derived for transpiration cooling with a laminar boundary layer on the hot-gas side (refs. 6 and 7). Approximate solutions for turbulent boundary-layer flow are given in references 8 and 9. Some preliminary calculations based on previous work indicate substantially lower cooling-air requirements for a transpiration-cooled afterburner than

for one using convective cooling. Since insufficient information existed on which to base precise theoretical calculations, the construction and evaluation of a full-scale porous-wall afterburner was undertaken. It was believed that this investigation would permit rapid discovery of solutions to design problems and answers to questions arising from this method of cooling afterburners.

2833

The first problem was the selection of a porous material having the requisite air-flow characteristics and strength at temperatures up to 1100° F. The second and related problem was the design and fabrication of the porous wall so that it would safely withstand the collapsing forces imposed by the pressure drop across the porous material. A foremost question was the susceptibility of the porous material to clogging by dust and foreign particles in the cooling-air supply or to deposits of soot or fuel residues on the hot-gas side of the wall. Another question was the rate of oxidation at elevated temperatures and the influence of the oxidation products on the clogging of the porous material.

CF-1 back

This report presents the results of a preliminary investigation of a combustion-chamber wall fabricated from commercially available, sintered, porous stainless steel; discusses some of the design and fabrication problems that may occur with this method of afterburner cooling, and provides data for further evaluating the potentialities of this method of cooling.

APPARATUS

Sintered, Porous Stainless-Steel Combustion-Chamber Wall

A preliminary search for suitable porous materials disclosed that no commercial product possessed all the desired properties, nor was one available in a form and size readily applicable to an afterburner combustion chamber. The compromise choice was sintered AISI type 304 porous stainless steel in plates 9 by 27 inches (maximum size available) and 1/4 inch thick. This thickness was selected so that the wall would sustain the pressure drop across it without external supports that might tend to disrupt the continuity of the air flow through the wall. This thickness also facilitated the installation of thermocouples within the wall.

Consideration of the increases in cooling requirements and in pressure drop across the porous wall with distance downstream of the flame holder led to the selection of three grades of porous stainless steel. These three grades were selected so as to vary the permeability along the length of the combustion chamber, in an effort to match somewhat the air flow to the estimated coolant requirements. The manufacturer's specifications for the three grades of material used are presented in table I.

The cylindrical combustion chamber (fig. 1) had an inside diameter of 25.5 inches and length of 58.5 inches from the flame-holder bolts to the exhaust-nozzle inlet, of which the last 54 inches was of porous material (fig. 2). The porous plates were rolled and hand-welded in a single pass by an inert-gas-shielded tungsten arc into the cylinder shown in figure 1. Roll-forming at a 12.75-inch radius of curvature had no measurable effect on the air-flow calibration of the porous materials. The porous cylinder was held concentric within the cooling shroud by eight spacer clips (see fig. 3) equally spaced around the circumference in each of three planes along the length. The upstream end of the porous wall was sealed by means of a bellows to allow for differential thermal expansion, and the cooling-air flow was restricted at the nozzle end of the porous wall by a labyrinth seal.

2833

Test Facility

The porous-wall afterburner was mounted on a conventional axial-flow turbojet engine installed in an altitude test chamber. The sea-level static thrust of the engine was approximately 3100 pounds at rated engine speed of 12,500 rpm and a maximum turbine-outlet temperature of approximately 1660° R. At this condition, the air flow was slightly less than 60 pounds per second. Figure 3 shows a sectional view of the afterburner assembly and details of the flame holder and fuel-spray system. The section between the turbine flange and the beginning of the porous wall, including the flame holder and fuel-spray bars, is identical with the high-performance afterburner configuration of reference 10, which evolved from configuration C of reference 2.

Cooling air was supplied from an independent source and flowed through 200 square feet of 1-inch-thick Fiberglas filter media. The maximum particle size passed was less than 1 micron. The air then flowed through an A.S.M.E. standard thin-plate orifice installation and pressure-regulating valve outside the altitude test chamber, entered a plenum chamber at the upstream end of the porous wall through two diametrically opposed inlet ducts, and flowed rearward through the $1\frac{9}{16}$-inch annular cooling passage and the porous wall into the combustion chamber.

Two convergent water-cooled exhaust nozzles having exit areas of 2.21 and 2.40 square feet were used.

The engine fuel was clear, unleaded gasoline of 62-octane rating, and the afterburner was operated with MIL-F-5624A, grade JP-4, fuel.

Instrumentation

The engine instrumentation was standard and identical with that of reference 10. The principal afterburner instrumentation was installed in the three planes A, B, and C shown in figure 2. The location of each temperature and pressure measurement on the porous wall is shown in figure 4(a), and on the afterburner cooling shroud in figure 4(b).

Details of the thermocouple installation in the porous wall are shown in figure 5. This type thermocouple installation offered a minimum disturbance to the flow of air through the wall and to the normal temperature profile across the wall. The thermocouples at the 270°, 315°, and 360° circumferential positions looking downstream and the combustion-gas static-pressure taps at the 22.5° circumferential position are visible in figure 1. The air temperature in the cooling passage was measured by butt-welded iron-constantan thermocouple probes (fig. 6).

TEST PROCEDURE

One data point was obtained at a simulated altitude of 36,700 feet and a flight Mach number of 0.81 with an exhaust-nozzle-throat area of 2.21 square feet. The rest of the data were obtained at a simulated altitude of 35,000 feet and a flight Mach number of 1.0 with exhaust-nozzle-throat areas of 2.21 and 2.40 square feet. The gas temperatures at the exhaust-nozzle exit ranged from 2858° to 3816° R, the turbine-discharge temperatures from 1420° to 1666° R, and the coolant-flow ratios from 0.032 to 0.154.

The cooling-air flow was varied over as wide a range as possible for several values of afterburner fuel flow. The minimum cooling-air flow was limited by maximum permissible wall temperature. Maximum cooling-air flows at high combustion-gas-temperature levels were limited by maximum turbine-discharge temperature, which increased with cooling-air flow for a given combustion-gas temperature because the fixed-area exhaust nozzles were choked.

CALCULATION PROCEDURE

Cooling-Air Flux Density

Local rates of cooling-air flow per unit area of the porous wall $(\rho v)_a$ were calculated from the local pressure drop across the wall, the local average wall temperature, and calibrations of the three grades of porous stainless steel. The calibration procedure and the method of generalizing the flow data were the same as used in reference 11. The

final calibration curves are shown in figure 7 for grades E, F, and G porous stainless steel used in the experimental afterburner and for an improved quality of porous stainless steel designated herein as grade H. (The physical properties of grade H porous stainless steel are presented in table II.) The ordinate of the calibration curve (fig. 7) is, in effect, a measure of the pressure drop per unit thickness across the porous wall $\frac{\Delta(p^2)}{\tau}\left(\frac{\mu_o}{\mu}\right)^2\frac{T_o}{T}$, and the abscissa is the generalized weight flow per unit area $(\rho v)_a\,\mu_o/\mu$ normal to the porous wall. (Symbols are defined in appendix A.) The viscosity and temperature ratios reduce the air-flow data to standard temperature. It is shown analytically in reference 12 that the temperature of the air within the porous wall differs from the local metal temperature by a fraction of a degree, except for a very short distance where the air enters the wall. Consequently, the viscosity in the factors μ_o/μ and $\left(\frac{\mu_o}{\mu}\right)^2\frac{T_o}{T}$ (fig. 8) was evaluated at the local average wall temperature measured 3/16 inch from the air side of the wall.

2833

Cooling-Air Flow

The cooling-air flows measured by means of the A.S.M.E. thin-plate orifice were not used in determining the values of coolant-flow ratio $W_a/W_{g,8}$ reported herein, because cracks appeared along some of the welded seams in the porous wall and permitted part of the measured air flow to leak into the combustion chamber without being utilized as a coolant. Consequently, the coolant-flow ratios are based on cooling-air flow calculated from a step-by-step integration of the cooling-air flux density $(\rho v)_a$ over the entire area of the porous wall.

Varying degrees of oxidation developed in the porous stainless-steel wall during the course of the investigation. This oxidation resulted in a gradual reduction in local cooling-air flows through the oxidized areas from those calculated from the air-flow calibration curves for new materials. The partial reduction in cooling-air flows through the oxidized areas in the G and F grades of porous stainless steel was ignored in integrating the total effective cooling-air flow through the porous wall. Only a slight error resulted, because the entire air flows through new G and F grade materials used in the wall were, respectively, 1 and 6 percent of the total cooling-air flow.

Correlation of Temperatures on Porous Wall

The temperature-difference ratio $\frac{T_w - T_a}{T_g - T_a}$ and its related parameter $\frac{T_g - T_w}{T_g - T_a}$ have been used by earlier investigators to correlate the temperature of a porous material with the temperature of the combustion gas and cooling air. The data for a porous turbine blade are correlated (ref. 4) by plotting $\frac{T_w - T_a}{T_g - T_a}$ against the ratio of the cooling-air flux density normal to the porous wall to the total gas flow per unit of combustion-gas-flow area $\frac{(\rho v)_a}{(\rho U)_g}$. Canright (ref. 3) and Wheeler (ref. 13) have plotted, in the notation of this report, $\frac{T_g - T_w}{T_g - T_a}$ against $\frac{(\rho v)_a}{(\rho U)_g}$ for a porous wall section in a rocket combustion chamber. The ratio $\frac{T_g - T_w}{T_g - T_a}$ has been correlated against the parameter $\left(\frac{v_a}{U_g}\right)^2 Re$ in reference 14, where Re is the Reynolds number relating to the flow conditions in the main stream. The data in this report are correlated in the same manner as in reference 4.

The combustion-gas bulk total temperature $T_{g,x}$ at any distance x downstream of the flame holder was obtained from the empirical equation (ref. 15)

$$\frac{T_{g,x} - T_{g,0}}{T_{g,8} - T_{g,0}} = \sin \frac{\pi}{2} \frac{x}{L} \qquad (1)$$

where

$T_{g,0}$ total temperature at burner inlet, $^{\circ}R$

$T_{g,8}$ total temperature at exhaust-nozzle exit, $^{\circ}R$ (appendix B)

L distance from flame holder to exhaust-nozzle exit

The value of $T_{w,g}$ used in the correlation parameters of this report is the local average surface temperature on the hot-gas side of the porous wall. The temperature $T_{w,g}$ was obtained from the equation

$$T_{w,g} = T_{w,3/16} + \Delta T \qquad (2)$$

where $T_{w,3/16}$ is the circumferential average of local wall temperatures measured at a depth of 3/16 inch from the air-side of the porous wall, and ΔT is the average difference between local wall temperatures measured by the flush gas-side thermocouples and the thermocouples imbedded at 3/16-inch depth at the 135° and 315° circumferential positions. The values of ΔT ranged from about 15° to 80° R.

2833

In averaging the wall temperatures, it was necessary to omit those values obtained in regions where severe oxidation had occurred. Peak wall temperatures of 1475° F appeared at the 0° and 180° circumferential positions of station B when the afterburner was first lighted. Brown to purple-black oxidized areas coinciding with the peak temperatures at station B were observed on the inside surface of the porous wall upon inspection after 2 hours of afterburning. Subsequent checks revealed that the oxidation had been severe enough to nullify the air-flow calibration in these areas. Temperature measurements by thermocouples located in badly oxidized areas at station B were therefore omitted from the circumferential average temperature used in correlating $\frac{T_{w,g} - T_a}{T_g - T_a}$ against $\frac{(\rho v)_a}{(\rho U)_g}$. Fortunately, the thermocouples at the 135° and 315° circumferential positions of station B were not in badly oxidized regions of the porous wall.

Optimum Cooling-Air Flow

The optimum longitudinal distribution of cooling air and the resultant coolant-flow ratios were calculated for several constant values of wall temperature from the experimental correlation of $\frac{T_{w,g} - T_a}{T_g - T_a}$ against $\frac{(\rho v)_a}{(\rho U)_g}$ for this afterburner. A knowledge of the actual distributions of permeability or thickness of any specific porous material and of the cooling-air pressure is not necessary for these calculations, so long as the values of $\frac{(\rho v)_a}{(\rho U)_g}$ or $(\rho v)_a$ obtained from the correlation for a given set of temperature and gas-flow conditions are maintained. The corresponding coolant-flow ratios were obtained for the combustion-chamber geometry of this investigation from a step-by-step integration of the optimum distribution $(\rho v)_a$ over the whole porous surface.

2833

CF-2

RESULTS AND DISCUSSION

Typical Temperature and Pressure Profiles

Typical circumferential temperature profiles of the cooling air and porous wall are presented in figure 9. Temperature peaks were observed at the 0° and 180° circumferential positions for stations A and B, and to a lesser extent for station C. Generally, the differences between the maximum and minimum wall temperatures at stations A, B, and C, respectively, were about 200° to 300° F, 500° to 700° F, and 30° to 100° F. The cooling at station C was especially effective, in spite of high combustion-gas temperatures, as evidenced by average temperature differences between the wall and the cooling air of 20° to 100° F. This low temperature rise indicated an excessive and wasteful use of cooling air.

Typical temperature profiles across the porous wall are shown in figure 10. This temperature profile was shown analytically to be a gradual exponential curve in reference 12. The large degree of overcooling at station C is quite apparent from a comparison of the temperatures of the wall and the cooling air.

Typical longitudinal distributions of static pressure in the cooling passage and inside the combustion chamber are shown in figure 11. There was negligible drop in pressure along the cooling passage because of its large height, but the drop in combustion-gas pressure increased with increases in the heat released by combustion.

It will be observed from the shape of the static-pressure curves in figure 11 that the pressure drop across the porous wall $p_a - p_g$ could become zero or negative near the flame-holder end of the porous wall with reduced cooling-passage pressure, while a positive pressure drop across the wall farther downstream might be large enough to cause local overcooling of a high-permeability wall. Such a condition could be averted if the cooling-air pressure were raised to provide an adequate insulating air film on the porous surface near the flame holder with a simultaneous reduction in the permeability of the porous wall in the downstream region. For a given coolant flow, the selection of lower-permeability porous materials will increase the required coolant pressure and, in general, tend to decrease the percentage variation in pressure drop across the wall with distance from the flame holder in comparison with the average pressure drop across the wall. A compromise is necessary, because high pressure drops imply heavier structure to support the wall against the larger pressure forces.

Correlation of Wall Temperatures

The temperature-difference ratio $\frac{T_{w,g} - T_a}{T_g - T_a}$ and the ratio $\frac{(\rho v)_a}{(\rho U)_g}$ were evaluated for each data point at stations A, B, and C and plotted against each other in figure 12 to give the experimental cooling correlation for this afterburner. A well-defined curve resulted for the data obtained from all three grades of porous stainless steel over a range of gas temperatures from about 1700° to 3700° R and combustion-gas flows, at the flame holder, of 20.6 and 28.5 pounds per second. The correlation curve applies to the data obtained at the high altitude conditions of this investigation where the combustion flames were nonluminous.

The correlation obtained from this investigation is compared in figure 13 with the experimental correlations obtained for an air-cooled, sintered, porous stainless-steel turbine blade (ref. 4) and for a nitrogen-cooled, porous section just upstream of the nozzle in a liquid-fuel rocket (ref. 16, p. 318). The agreement between the correlations of the three investigations is considered good. If the assumption is made that turbulent boundary-layer flow existed in each investigation, the spread between the curves can be accounted for approximately by the variation in Reynolds number among the investigations. The large apparent spread between the curves at low values of temperature-difference ratio is actually the result of only small differences in wall temperature. For instance, for a temperature difference of 2000° R between the gas and cooling air, the maximum spread in the curves at a flux density ratio of 0.025 results in less than 100° R variation in the wall temperature.

Distribution of Cooling-Air Flux Density

The longitudinal distribution of cooling-air flux density $(\rho v)_a$ in this afterburner was calculated for several data points from static-pressure curves similar to figure 11, the correlation curve (fig. 12), and the calibration of the three grades of porous stainless steel (fig. 7). An iterative procedure was used, because the longitudinal distribution of wall temperature was necessary to evaluate the viscosity factors in determining $(\rho v)_a$ from the air-flow calibration curves, and the wall temperatures were dependent on $(\rho v)_a$. Typical distributions of $\frac{(\rho v)_a}{(\rho U)_g}$ (and hence $(\rho v)_a$, since $(\rho U)_g$ is approximately constant

for a given combustion-gas flow) are shown in figure 14. The combination of low permeabilities and small pressure drops across the wall, together with increased air viscosity resulting from the high wall temperatures, permitted little air to flow through grades G and F porous stainless steel. By coincidence, the effect of increasing pressure drop on cooling-air flux density was counterbalanced by increasing air viscosity effects, so that $\frac{(\rho v)_a}{(\rho U)_g}$ or $(\rho v)_a$ was practically independent of distance in the G and F grade material. In contrast $(\rho v)_a$ increased with distance from the flame holder in the grade E material, because the static-pressure drop across the wall increased as the static pressure in the combustion chamber decreased. It will be shown later that the wall temperature, and hence the temperature and viscosity of the cooling air flowing through the grade E material, was practically independent of distance from the flame holder.

CF-2 back

Longitudinal Distribution of Cooling Air

Typical curves of the fraction of the total cooling-air flow that passed through the porous wall are plotted against the distance from the flame holder in figure 15. Discontinuities occurred in the curves at the junctions of different grades of porous material; however, changes in coolant-flow ratio or combustion-gas-temperature level over the ranges investigated had only a slight effect on the longitudinal distribution of cooling air. The cooling air that passed through grades G, F, and E porous stainless steel, respectively, were about 1, 6, and 93 percent of the total cooling-air flow.

Longitudinal Distribution of Wall Temperature

The calculated longitudinal temperature distributions for the combustion gas (eq. (1)) and for the hot-gas surface of the porous wall (based on the correlation curve of fig. 12) are presented in figure 16 with the longitudinal distribution of average cooling-air temperature. The temperatures measured by the thermocouples imbedded 3/16 inch from the air side of the wall are also plotted at stations A, B, and C. A coolant-flow ratio $W_a/W_{g,8}$ of 0.042 and an exhaust-gas temperature of 2858° R (fig. 16(a)) resulted in peak wall temperatures of 1330° and 1370° R, respectively, at stations A and B. The calculated wall temperatures based on the experimental correlation were nearly constant in the grade E material, with a value of 860° R at station C. A similar curve (fig. 16(b)) resulted with a coolant-flow ratio of 0.107 at an exhaust-gas temperature of 3798° R. The calculated average wall temperatures $T_{w,g}$ at stations A, B, and C were, respectively, 1440°,

1390° , and 670° R. These temperatures are all below 1560° R, which is considered to be about the maximum allowable average temperature, from strength and oxidation considerations, for the porous material in this afterburner. These low temperatures illustrate the high cooling effectiveness provided by transpiration air-cooling. The coolant-flow ratios would have been considerably lower, if several grades of porous material intermediate between E and F had been available to provide an effective matching of cooling-air flux density to the required densities.

The agreement between the measured and calculated temperatures is excellent for figure 16(a). The agreement is fair for stations A and C in figure 16(b), where the data were taken after a total of 6 hours of afterburner operation. The poorest agreement was at station B, where the grade F porous stainless steel developed hot spots and began to oxidize early in the investigation. These oxidized regions extended with time, and the clogging gradually became more severe. Consequently, the actual flux density in this region was nonuniform and averaged out to less than that calculated from the calibration curve for new material.

2833

Effect of Permeability on Cooling-Air Requirements

The results of figure 16 suggest that the cooling air would be more effectively utilized if the permeability were varied so as to maintain a constant wall temperature along the length of the combustion chamber. In actual practice, the variation of permeability and the cooling-air pressure to obtain a constant wall temperature would be affected by the choice of flight plan and by afterburner operating parameters. The criteria for selecting the design point to obtain the best compromise distribution of permeability and cooling-air pressure are beyond the scope of this report.

The curves of figure 17 show the optimum distribution of cooling air for three values of constant wall temperature for the same test conditions as for figure 16(b). The cooling-air distribution for constant wall temperature shows the simultaneous reduction in the rate of coolant addition in the upstream region and the increasing rate of coolant addition in the downstream region of the porous wall as the wall temperature level is increased. For an exhaust-gas total temperature of 3798° R, a burner-inlet total temperature of 1656° R, an inlet cooling-air temperature of 533° R, and a combustion-gas flow at the flame holder of 29.1 pounds per second (0.057 pound per second per square inch of burner flow area), the ideal minimum coolant-flow ratios for constant wall temperatures of 680°, 1415°, and 1560° R are, respectively, 0.131, 0.022, and 0.016. The value of 0.016 is only 8 to 11 percent of the coolant-flow ratios required to maintain an average maximum wall temperature of 1760° R under similar operating conditions for a solid-wall forced convection cooled by air flowing through a 1/2-inch annular cooling shroud.

For comparison, and to illustrate the characteristics of some actual porous materials, the distributions of temperature (fig. 18(a)) and of cooling air (fig. 18(b)) were calculated by means of the correlation (fig. 12) for the combustion-chamber wall fabricated from porous stainless steel of uniform permeability because of the design simplicity and ease of fabrication of this material. The distributions of temperature and of cooling-air flow shown are those that would result, with the conditions of figure 16(b), if the combustion chamber was fabricated from 1/4-inch-thick plates of grades E, F, and G porous stainless steel or from 0.034-inch-thick grade H improved quality porous stainless steel. A constant wall temperature was approached by the grade E material (fig. 18(a)), for which the longitudinal profile of wall temperature approximated the temperature profile of the cooling air. The wall of grade E material is overcooled. Correspondingly, the coolant-flow ratio is high (0.133), although it is close to the ideal minimum value of 0.131 for a constant wall temperature of 680° R, since the initial and final wall temperatures are, respectively, 630° and 690° R.

The less permeable grades of porous material produce proportionately higher wall temperatures, with trends that approximate the combustion-gas temperature. As a result, the upstream region of the porous wall is cooler than the maximum temperature in a given grade of material, and the coolant-flow ratios become increasingly greater than the ideal minimum for a constant-temperature wall having the same temperature limit, as the wall temperature level is increased. For instance, a coolant-flow ratio of 0.032 is necessary to obtain a maximum wall temperature of 1415° R in the grade F material; whereas the ideal minimum coolant-flow ratio is only 0.022 for a constant wall temperature of 1415° R. Large areas of walls made from either grade G or H would be overheated at a cooling-air pressure of 12.36 pounds per square inch absolute. However, a pressure increase from 12.36 to 12.50 pounds per square inch absolute would give a maximum temperature of 1560° R and a coolant-flow ratio of 0.037 in the grade H material. This coolant-flow ratio is more than double the ideal minimum of 0.016 for a constant wall temperature of 1560° R for the previously mentioned temperatures and combustion-gas flow per unit area. For the operating conditions discussed in the preceding illustration, the cooling-air requirements are approximately 50 to 100 percent greater than for walls having ideal permeability distribution.

The longitudinal distributions of cooling-air flow for combustion chambers fabricated of uniform-permeability porous stainless steel are shown in figure 18(b) along with the optimum cooling-air distribution for a constant wall temperature of 1560° R. In the first 24 inches downstream of the flame holder, the coolant additions with uniform permeability are approximately 3.8 to 14 times the ideal addition for a constant wall temperature of 1560° R, as the maximum wall temperature is decreased from 1415° to 690° R for the operating conditions listed.

Fabricating and Operating Problems

Welding of the sintered, porous stainless steel was extremely difficult. The edges of the plates were machined square before welding, because beveled edges and weld penetrations greater than about 50 percent caused the material to crumble during welding. The welds were weakened because of oxidation of the porous metal at the interface between the metal and the weld bead. It is believed that sounder welds would have resulted if machine welding had been employed. Higher current densities and faster welding speeds, together with copious flooding with inert gas, would have resulted in less heating of the adjacent plate and reduced likelihood of oxidized metal at the interface between the porous plate and the weld bead.

Cracks developed in the oxidized regions adjacent to several welds from overheating and thermal stresses where the conductive cooling and the insulating effect of the transported air film were not large enough to cool adequately the impermeable weld beads (fig. 19). In addition to the discontinuities in the air film caused by welds, the film thickness varied because of nonuniformities in permeability and in thickness of the porous stainless-steel plates as received from the manufacturer. These variations in film thickness, together with possible hot streaks in the combustion gas, contributed to hot spots in the porous metal which developed into the oxidized regions shown in figure 19. One whole plate (fig. 19(a)) among the grade E porous stainless steel was severely oxidized in the first 2.2 hours of afterburning. A subsequent check disclosed that the plate was actually grade F material that had been mismarked grade E by the manufacturer. This piece and two smaller but heavily oxidized areas were replaced with new porous stainless steel before continuing the tests. After this initial period of operation, about 40 percent of the grade F material was moderately oxidized and about 30 percent of the grade G material was lightly oxidized.

The extent of the oxidized areas at the conclusion of the investigation, after 6.2 hours of afterburner operation, is shown in figure 19(b). About 70 percent of the grade G material was lightly oxidized, and about 80 percent of the grade F material was moderately or heavily oxidized. Scattered oxidized areas in the grade E material were generally adjacent to weld areas, except for a zone straddling the top center line in the wake of the heavily oxidized region of the grade F material. The high temperatures and oxidation in this zone were probably due to a hot streak in the combustion gas. The area of the most extensive and severe oxidation in the grade F and adjacent grade E material corresponds to the region of combustion-gas impingement on the wall, as indicated in reference 1. It seems probable that thin spots in the cooling-air film due to previously mentioned causes, coupled with the scrubbing and mixing of the hot gases at these spots, raised the local metal temperatures enough to accelerate oxidation and start the cycle

of events leading to severe oxidation and broken welds. Better design practice and improved fabricating techniques of more nearly uniform porous materials, together with the elimination of possible hot streaks in the combustion gas, can, no doubt, eliminate oxidation as a problem; but it may be necessary to provide a thicker air film than is indicated by the correlation curve herein to counteract turbulent mixing in the region of combustion-gas impingement.

The cooling-air pressure was always maintained high enough to ensure the flow of some cooling air through the entire porous surface, even during engine starting. No plugging of the porous material was evident except the oxidation that has been discussed. There were no deposits of soot or residues from the JP-4 fuel on the porous wall, even where the temperatures were 175° to 200° F (grade E), although the surfaces of the water-cooled tail rake at approximately the same temperatures became coated with a hard carbonaceous deposit.

CONCLUDING REMARKS

The application of transpiration cooling with air to the sintered, porous stainless-steel combustion-chamber wall of an afterburner was investigated experimentally. The temperatures of the hot-gas surface of the porous wall at three stations downstream of the flame holder were successfully correlated in terms of the local temperatures of the combustion gas and cooling air against the ratio of the cooling-air flux density normal to the porous wall to the combustion-gas flow per unit of combustion-chamber flow area. The correlation obtained from this afterburner is in good agreement with similar experimental correlations obtained for an air-cooled, sintered, porous turbine blade of stainless steel and for a nitrogen-cooled, porous section of a rocket combustion chamber.

Calculations based on the experimental correlation of this investigation indicate that for an exhaust-gas total temperature of 3798° R, a burner-inlet total temperature of 1656° R, an inlet-air temperature of 533° R, and a combustion-gas flow of 0.057 pound per second per square inch of burner flow area at the flame holder, a constant wall temperature of 1560° R can be maintained by transpiration cooling for a coolant-flow ratio of 0.016. This coolant flow is only 8 to 11 percent of that required to maintain an average maximum wall temperature of 1760° R under similar operating conditions for a solid-wall forced convection cooled by air flowing through a 1/2-inch annular cooling shroud. Calculations also indicate that the transpiration-cooling requirements are more than doubled for this afterburner, if, rather than maintaining a uniform wall temperature, the walls are fabricated from a uniform-permeability material so that the maximum wall temperature is 1560° R.

Oxidation of the porous metal was a problem wherever the wall temperatures exceeded about 1600° R. Areas of decreased thickness in the insulative cooling-air film, attributed to nonuniformities in thickness and permeability of the porous metal and to possible hot streaks in the combustion gas, led to hot spots and oxidation of the porous metal. The most extensive and severe oxidation occurred in the region of combustion-gas impingement on the wall and adjacent to welds. Better design practice and improved fabricating techniques of more nearly uniform porous materials, together with the elimination or reduction of hot streaks in the combustion gas, can, no doubt, remove oxidation as a problem.

2833

Lewis Flight Propulsion Laboratory
National Advisory Committee for Aeronautics
Cleveland, Ohio

APPENDIX A

SYMBOLS

A	flow area, sq in.
C_d	coefficient of discharge
C_t	area coefficient of thermal expansion
g	gravity constant, 386 in./sec^2
L	distance from flame-holder center line to exhaust-nozzle exit, in.
m	mass-flow rate, (lb)(sec)/in.
P	total pressure, lb/sq in. abs
p	static pressure, lb/sq in. abs
$\Delta(p^2)$	difference between squares of the absolute pressures on either side of porous wall, $p_a^2 - p_g^2$, lb^2/in.^{4}
R	gas constant, lb-in./(lb)($^\circ$R)
Re	Reynolds number
T	temperature of a solid or total temperature of a gas, $^\circ$R
T_o	NACA standard temperature at sea level, 519° R
U	local average axial velocity in combustion chamber, in./sec
v	local cooling-air velocity normal to porous wall, in./sec
W	flow rate, lb/sec
x	distance from flame-holder center line, in.
μ	viscosity of air at temperature T, lb/(in.)(sec)
μ_o	viscosity of air at T_o, lb/(in.)(sec)
ρ	density, lb/cu in.
τ	thickness of porous material, in.

CF-3

Subscripts:

a	cooling air
g	combustion gas or combustion-gas side
w	wall
x	at distance x measured from flame-holder center line
0	where x is zero
8	exhaust nozzle
3/16	measured at a depth of 3/16 inch from the air side of the porous wall

REFERENCES

1. Koffel, William K., and Kaufman, Harold R.: Cooling Characteristics of an Experimental Tail-Pipe Burner with an Annular Cooling-Air Passage. NACA RM E51K23, 1952.

2. Conrad, E. William, and Campbell, Carl E.: Altitude Wind Tunnel Investigation of High-Temperature Afterburners. NACA RM E51L07, 1952.

3. Canright, Richard B.: Preliminary Experiments of Gaseous Transpiration Cooling of Rocket Motors. Prog. Rep. No. 1-75, Power Plant Lab., Proj. No. MX801, Jet Prop. Lab., C.I.T., Nov. 24, 1948. (AMC Contract No. W-535-ac-20260, Ord. Dept. Contract No. W-04-200-ORD-455.)

4. Schafer, Louis J., Jr., Bartoo, Edward R., and Richards, Hadley T.: Experimental Investigation of the Heat-Transfer Characteristics of an Air-Cooled Sintered Porous Turbine Blade. NACA RM E51K08, 1952.

5. Eckert, E. R. G., and Esgar, Jack B.: Survey of Advantages and Problems Associated with Transpiration Cooling and Film Cooling of Gas-Turbine Blades. NACA RM E50K15, 1951.

6. Eckert, E. R. G., and Livingood, John N. B.: Calculation of Laminar Heat Transfer Around Cylinders of Arbitrary Cross Section and Transpiration-Cooled Walls with Application to Turbine Blade Cooling. NACA RM E51F22, 1951.

7. Brown, W. Byron: Exact Solutions of the Laminar Boundary Layer Equations for a Porous Plate with Variable Fluid Properties and a Pressure Gradient in the Main Stream. Paper presented at First U. S. National Congress of Applied Mechanics (Chicago), June 11-16, 1951.

8. Rannie, W. D.: A Simplified Theory of Porous Wall Cooling. Prog. Rep. No. 4-50, Power Plant Lab., Proj. No. MX801, Jet. Propl. Lab., C. I. T., Nov. 24, 1947. (AMC Contract No. W-535-ac-20260, Ord. Dept. Contract No. W-04-200-ORD-455.)

9. Friedman, Joseph: A Theoretical and Experimental Investigation of Rocket-Motor Sweat Cooling. Jour. Am. Rocket Soc., no. 79, Dec. 1949, pp. 147-154.

10. Useller, James W., Harp, James L., Jr., and Fenn, David B.: Turbojet-Engine Thrust Augmentation at Altitude by Combined Ammonia Injection into the Compressor Inlet and Afterburning. NACA RM E52L19, 1953.

APPENDIX B

CALCULATION OF EXHAUST-GAS TEMPERATURE

The exhaust-gas temperature was calculated from the equation

$$T_{g,8} = \left(\frac{pA}{m\sqrt{gRT}} \right)_8^{-2} \left(\frac{p_8 A_8 C_d C_t}{W_{g,8} \sqrt{\frac{R_8}{g}}} \right)^2 \qquad \text{(B1)}$$

Values of the static-pressure parameter $\frac{pA}{m\sqrt{gRT}}$ for various values of specific-heat ratio γ and pressure ratios p/P were obtained from reference 17. The area A_8 was measured at room temperature in the plane of total- and static-pressure measurement $4\frac{5}{8}$ inches upstream of the exhaust-nozzle throat. A discharge coefficient C_d of unity was assumed, since the pressures were surveyed at the centroids of five equal annuli. The area thermal-expansion coefficient C_t was assumed to be unity because of negligible expansion of the water-cooled conical exhaust nozzle. The specific-heat ratio γ and the exhaust-gas constant R were calculated in the usual manner for the mixture of exhaust gas and cooling air at station 8 from the thermodynamic data of reference 18 and the assumption that the relatively small percentage of cooling air introduced through the porous wall did not enter into the combustion process, but acted only as a diluent after combustion was completed.

CF-3 back

11. Donoughe, Patrick L., and McKinnon, Roy A.: Experimental Investigation of Air-Flow Uniformity and Pressure Level on Wire Cloth for Transpiration-Cooling Applications. NACA RM E52E16, 1952.

12. Weinbaum, S., and Wheeler, H. L., Jr.: Heat Transfer in Sweat-Cooled Porous Metals. Prog. Rep. No. 1-58, Air Lab., Proj. No. MX121, Jet Prop. Lab., C.I.T., Apr. 8, 1947. (AMC Contract No. W-535-ac-20260, Ord. Dept. Contract No. W-04-200-ORD-455.)

13. Wheeler, H. L., Jr.: The Influence of Wall Material on the Sweat-Cooling Process. Prog. Rep. No. 4-90, Jet Prop. Lab., C.I.T., May 3, 1949. (Ord. Dept. Contract No. W-04-200-ORD-455.)

14. Moore, N. P. W., and Grootenhuis, P.: Sweat Cooling. The Engineer, vol. 189, no. 4909, Feb. 24, 1950, pp. 230-231.

15. Koffel, William K., and Kaufman, Harold R.: Empirical Cooling Correlation for an Experimental Afterburner with an Annular Cooling Passage. NACA RM E52C13, 1952.

16. Dunn, Louis G., Powell, Walter B., and Seifert, Howard S.: Heat-Transfer Studies Relating to Rocket Power-Plant Development. Roy. Aero. Soc. and Inst. Aero. Sci. Third Anglo-American Aero. Conf. (Brighton, England), Sept. 4-7, 1951, pp. 271-363.

17. Turner, L. Richard, Addie, Albert N., and Zimmerman, Richard H.: Charts for the Analysis of One-Dimensional Steady Compressible Flow. NACA TN 1419, 1948.

18. Huff, Vearl N., Gordon, Sanford, and Morrell, Virginia E.: General Method and Thermodynamic Tables for Computation of Equilibrium Composition and Temperature of Chemical Reactions. NACA Rep. 1037, 1951. (Supersedes NACA TN's 2113 and 2161.)

19. Keenan, Joseph H., and Kaye, Joseph: Gas Tables. John Wiley & Sons, Inc., 1948.

TABLE I. - MANUFACTURER'S SPECIFICATIONS OF SINTERED AISI TYPE 304 POROUS STAINLESS STEEL

Property	Specification for grade		
	E	F	G
Mean pore opening, in.	0.0015	0.0008	0.0004
Mean pore opening, microns	35	20	10
Minimum ultimate tensile strength[a], lb/sq in.	15,000	15,000	15,000
Approximate modulus of elasticity[a], lb/sq in.	15×10^6	15×10^6	15×10^6
Elongation minimum, percent	5	5	5
Porosity[b], percent	52	40	37

[a]At room temperature.

[b]Determined from samples by NACA Lewis laboratory. Tolerance on thickness over 1/8 inch is +0.048 inch, -0.015 inch.

TABLE II. - MANUFACTURER'S SPECIFICATIONS OF IMPROVED-QUALITY AISI TYPE 316 POROUS STAINLESS STEEL

Property	Specification
Ultimate tensile strength, lb/sq in.	35,000-55,000
Approximate modulus of elasticity, lb/sq in.	15×10^6
Elongation, percent	
Test Coupon	3-8
Calculated from minimum bending radius	8-12
Calculated from hydrostatic test	10-14
Porosity, percent	20-25
Minimum bending radius, in.	3-times thickness
Tolerance on thickness, in.	±0.002

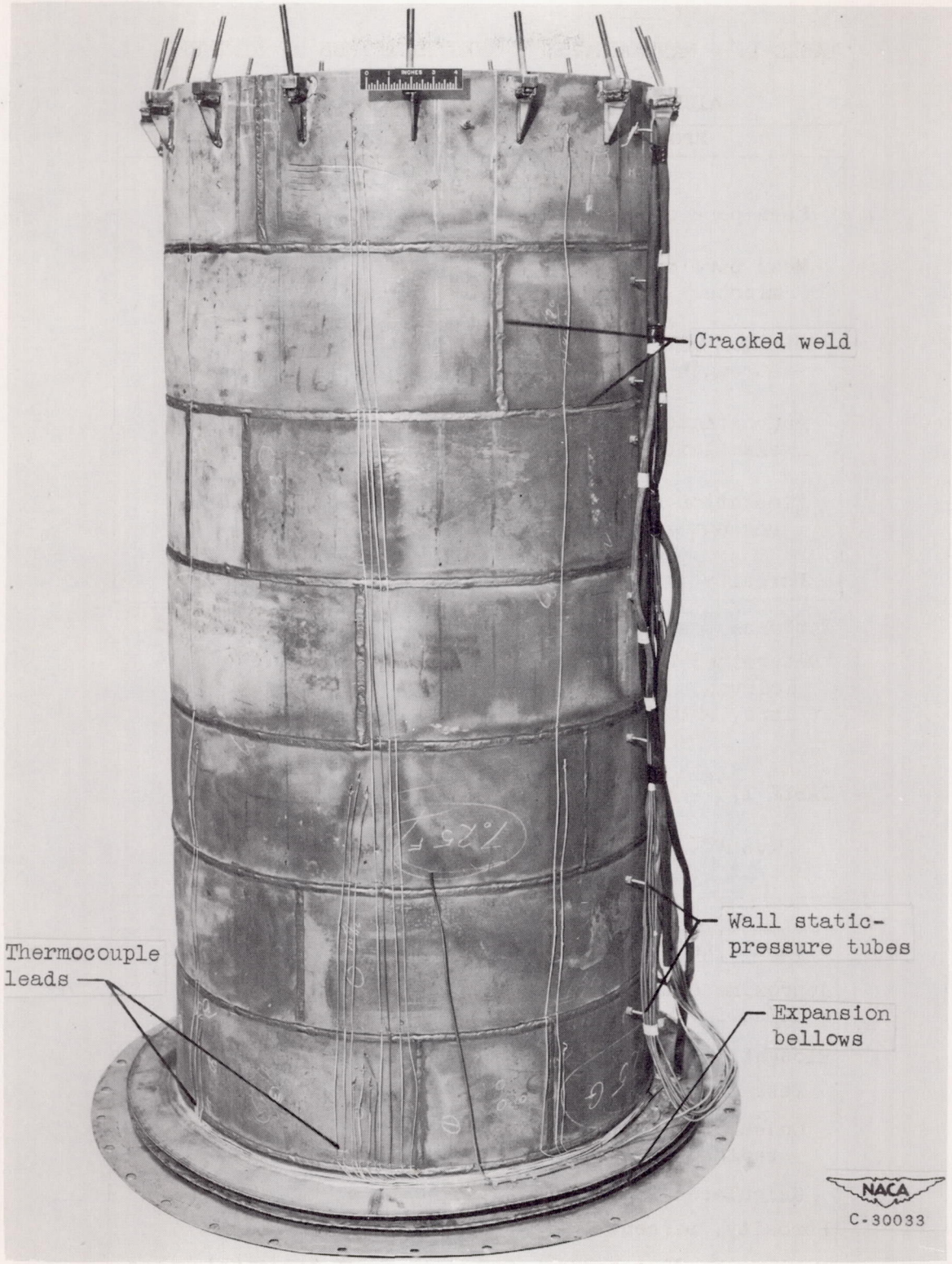

Figure 1. - Porous stainless-steel combustion-chamber wall after 2.2 hours of afterburning.

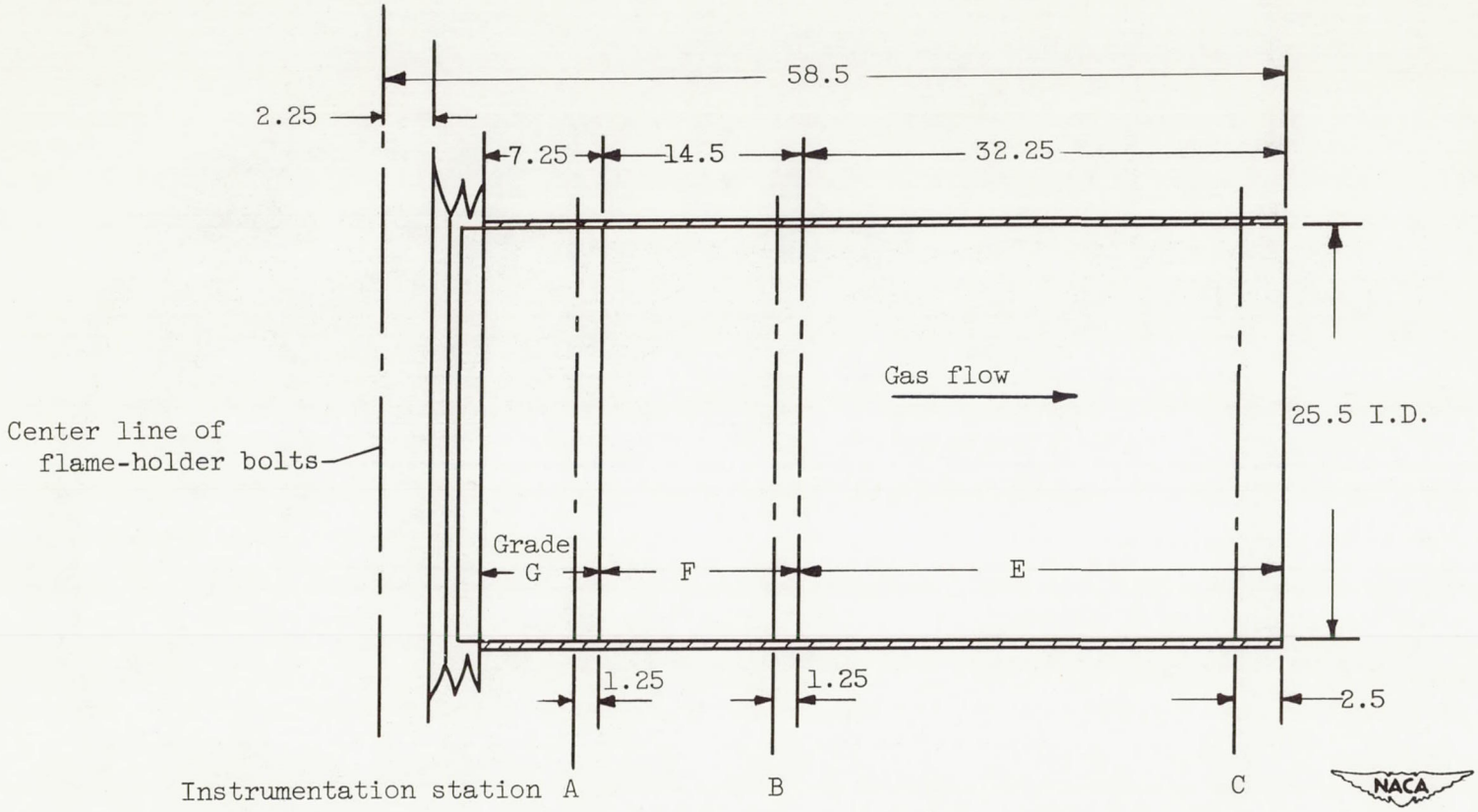

Figure 2. - Sketch of welded combustion-chamber wall of 1/4-inch-thick porous stainless steel showing instrumentation stations. (All dimensions in inches.)

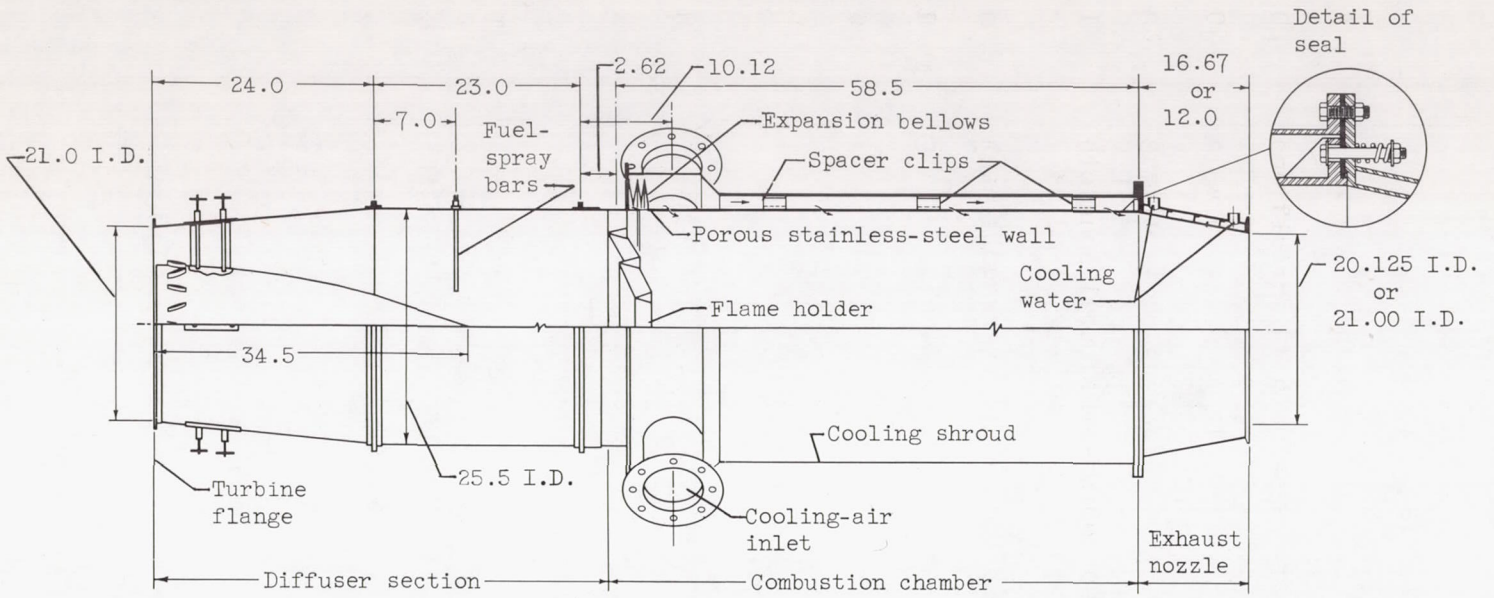

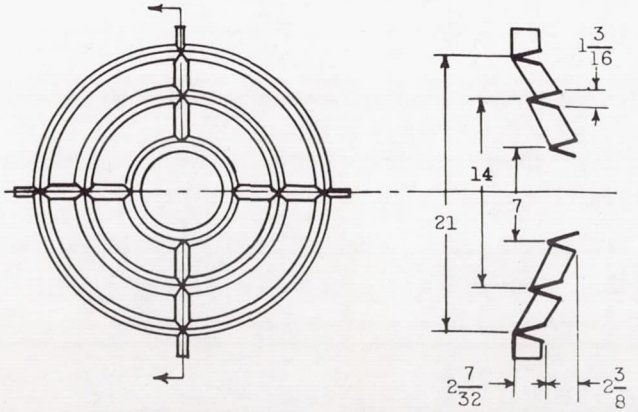

Flame holder; blockage, 35 percent

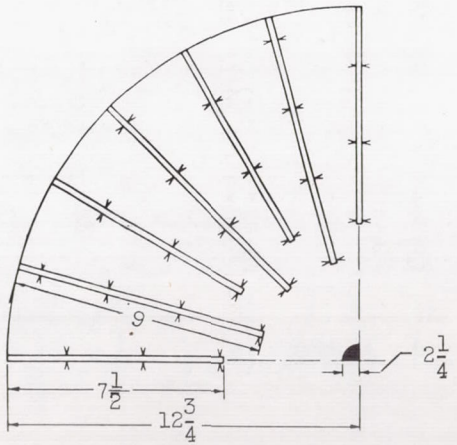

Fuel-spray system

Figure 3. - Sectional view of afterburner. (All dimensions in inches.)

NACA
CD-3021
CD-2885

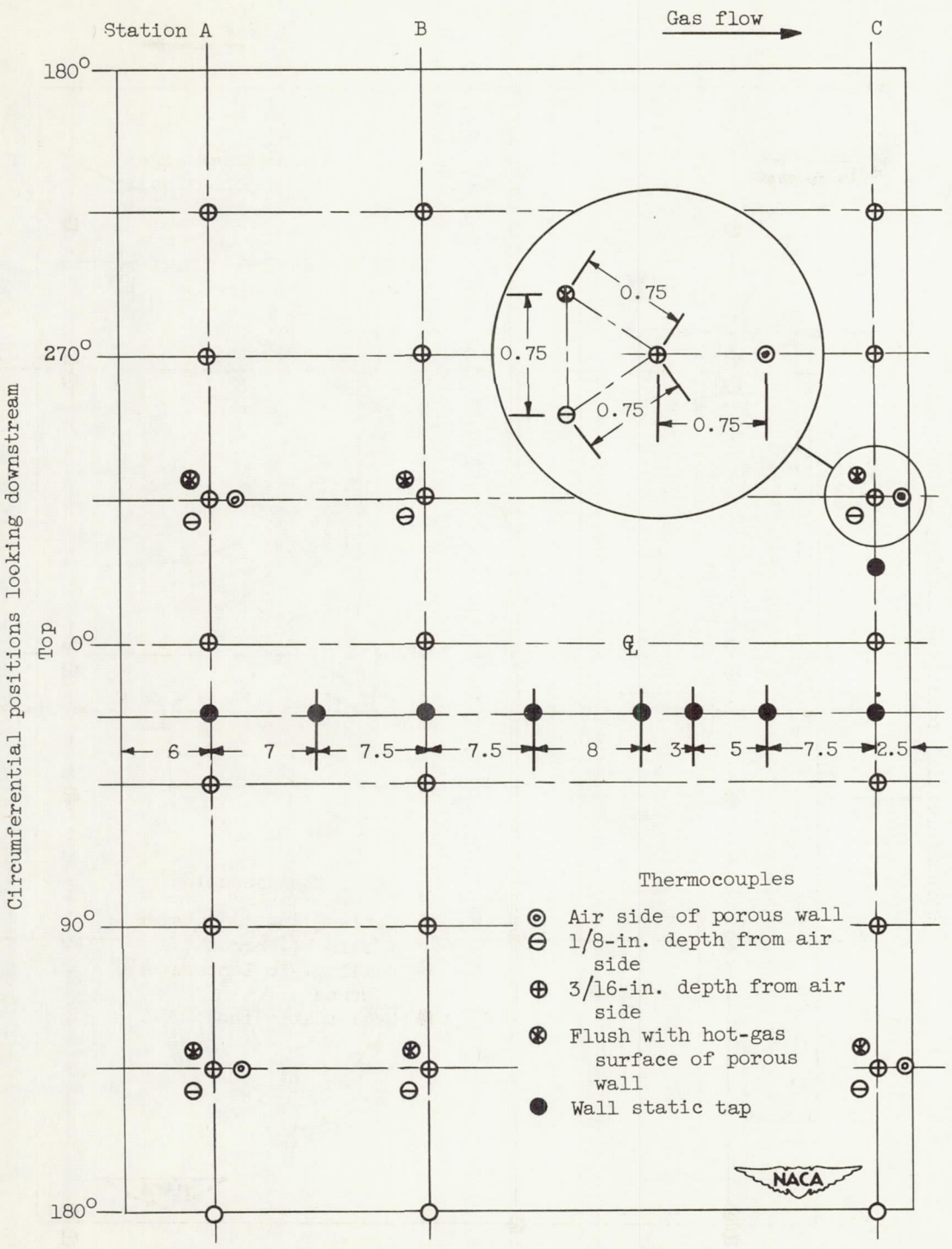

(a) Instrumentation on porous stainless-steel wall.

Figure 4. - Types and locations of afterburner instrumentation. (All dimensions in inches.)

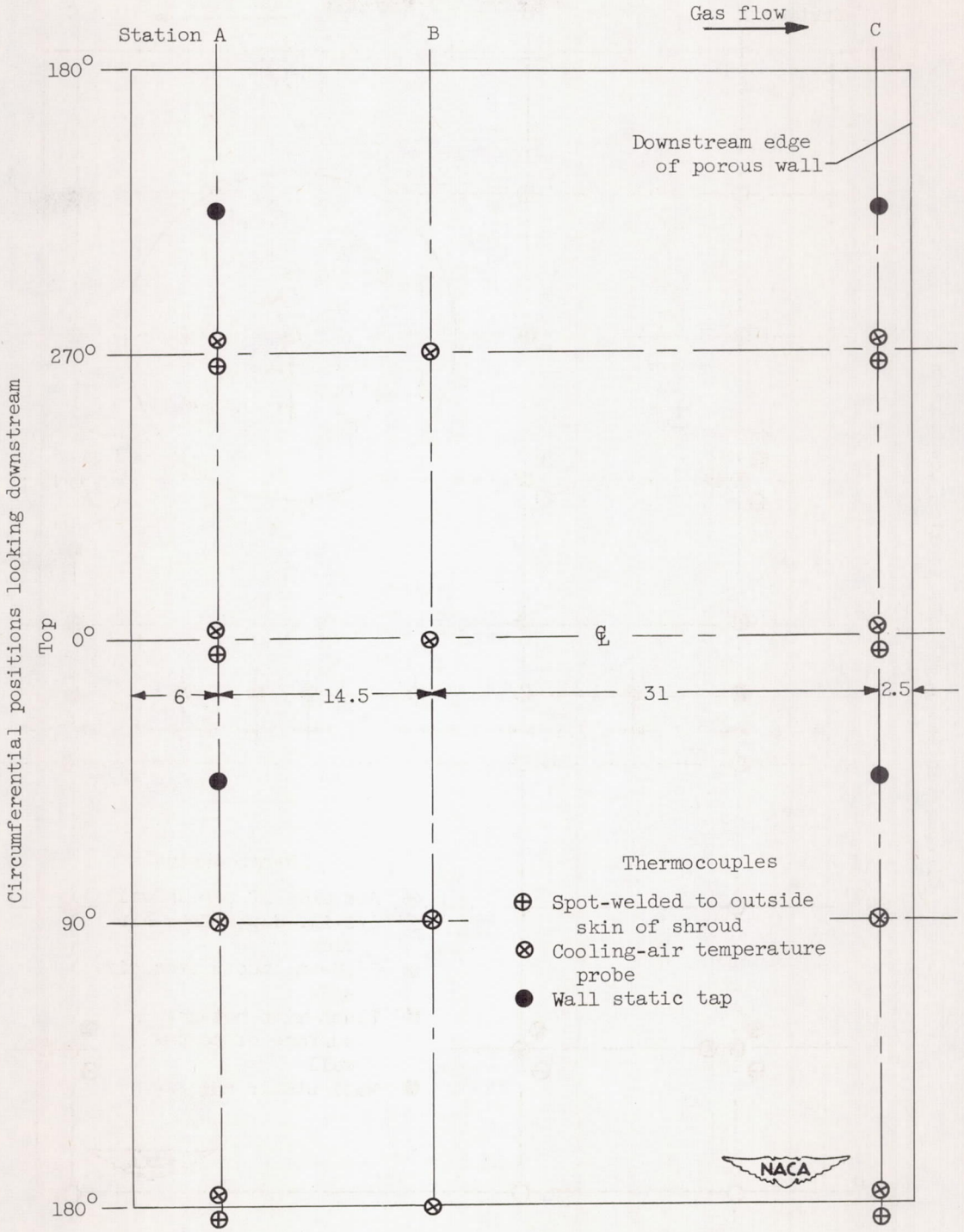

(b) Instrumentation on cooling shroud.

Figure 4. - Concluded. Types and locations of afterburner instrumentation. (All dimensions in inches.)

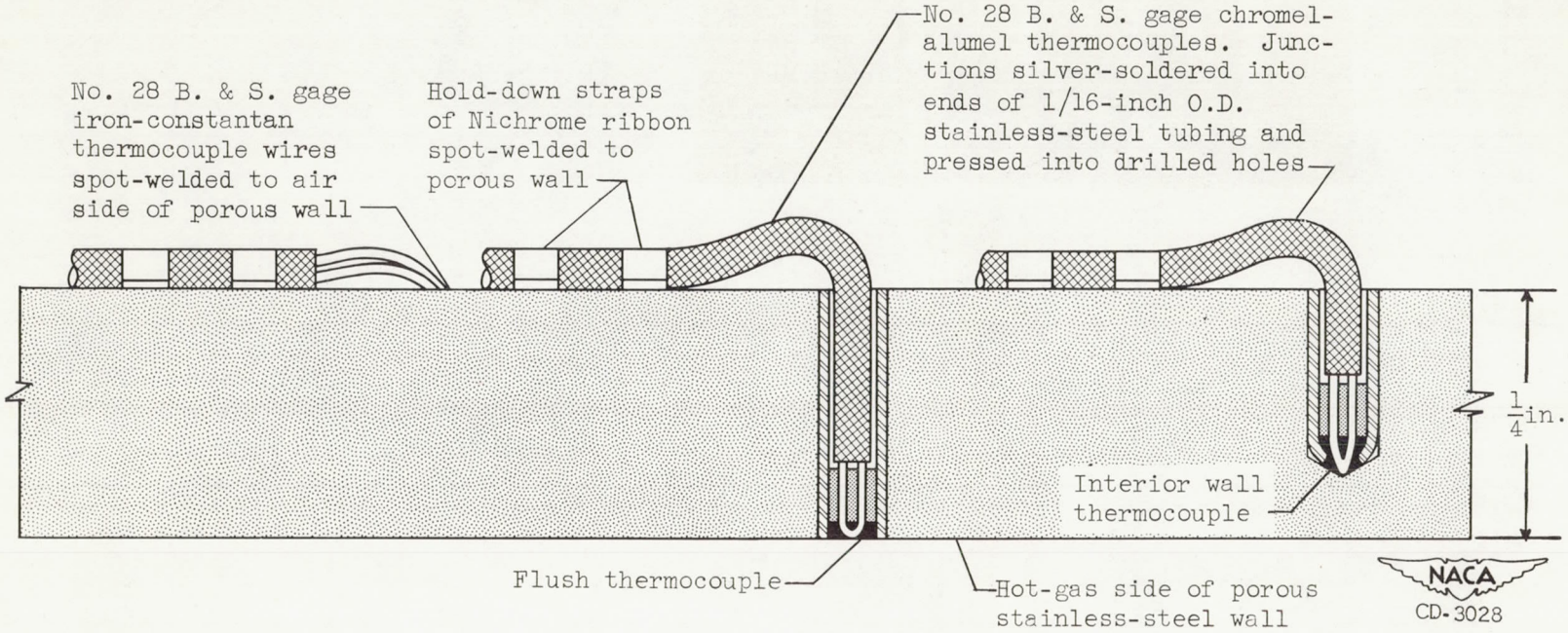

Figure 5. - Sectional view of typical thermocouple installations on porous stainless-steel wall.

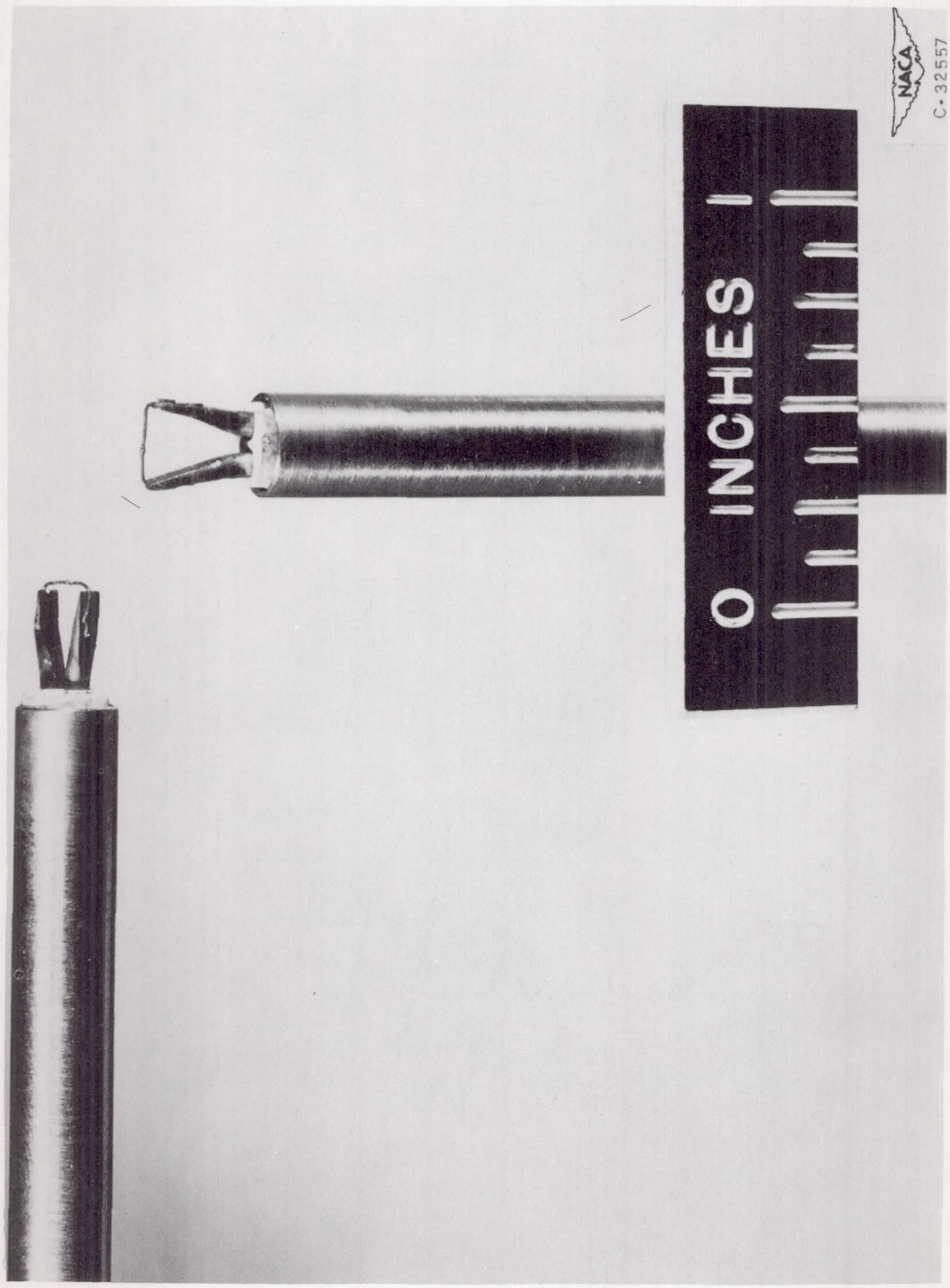

Figure 6. - Cooling-air thermocouple probe.

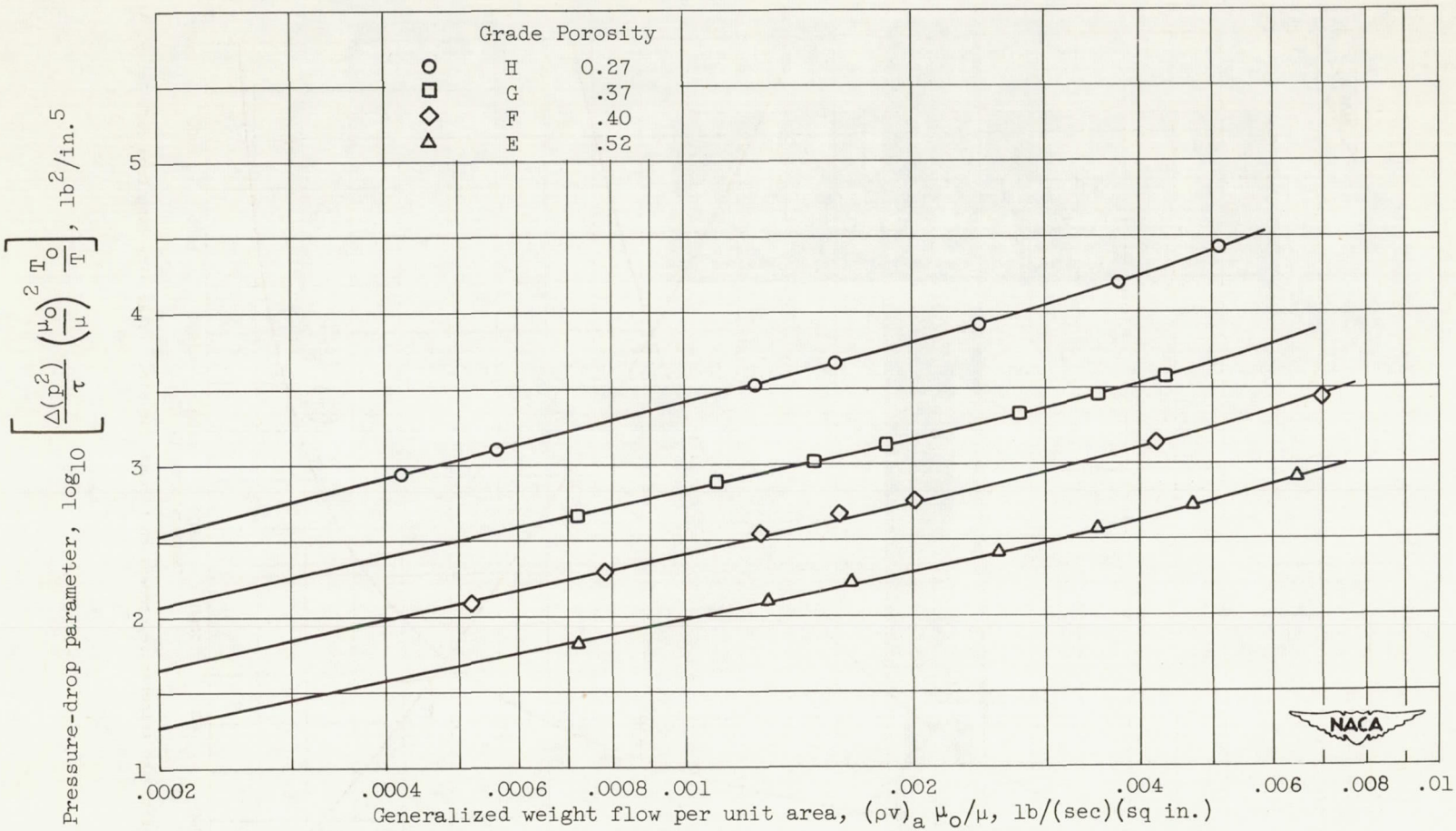

Figure 7. - Air-flow calibrations for sintered, porous stainless-steel wall material reduced to standard temperature.

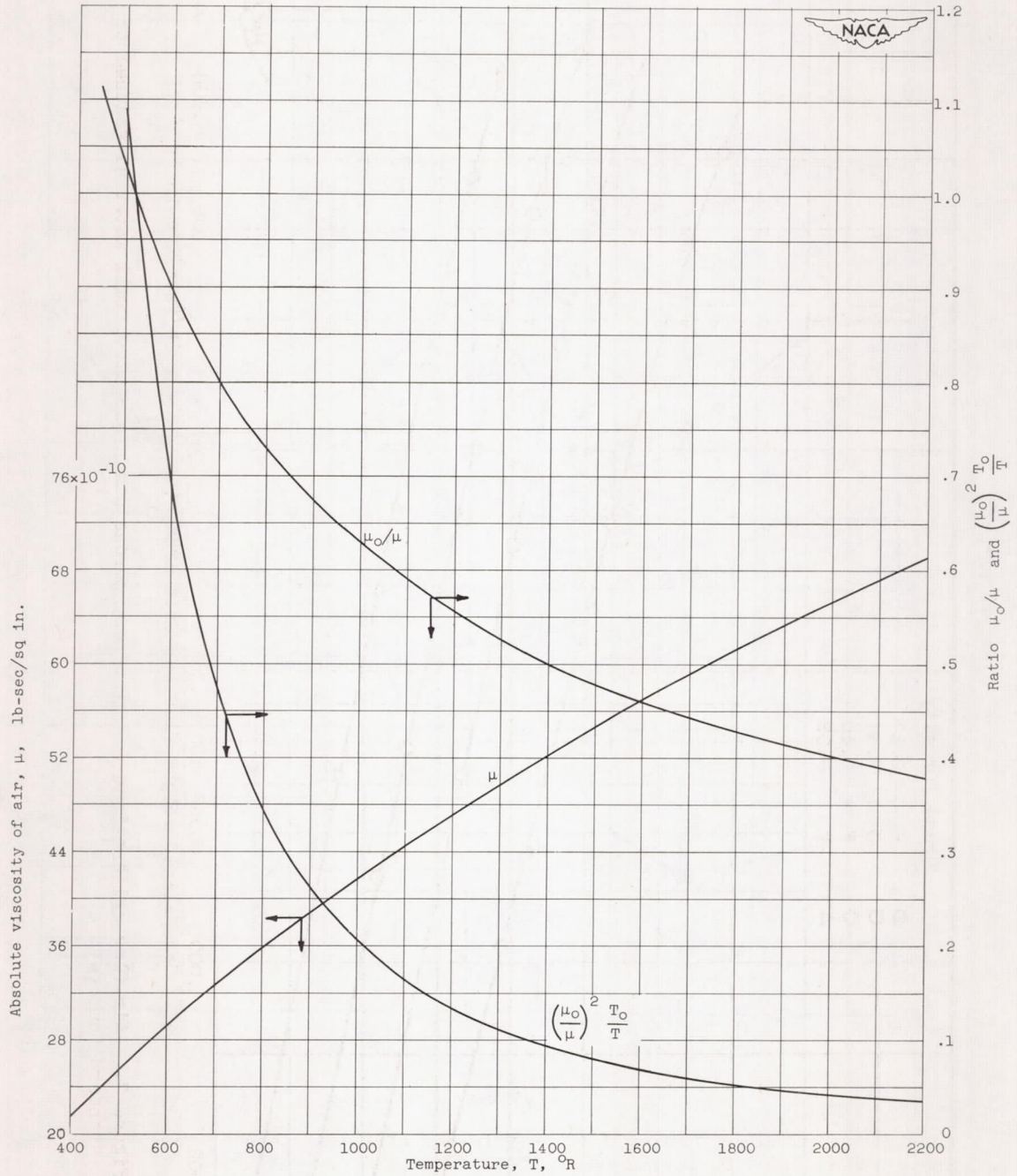

Figure 8. - Viscosity and temperature correction factors for air. (Viscosity data from ref. 19, p. 34.)

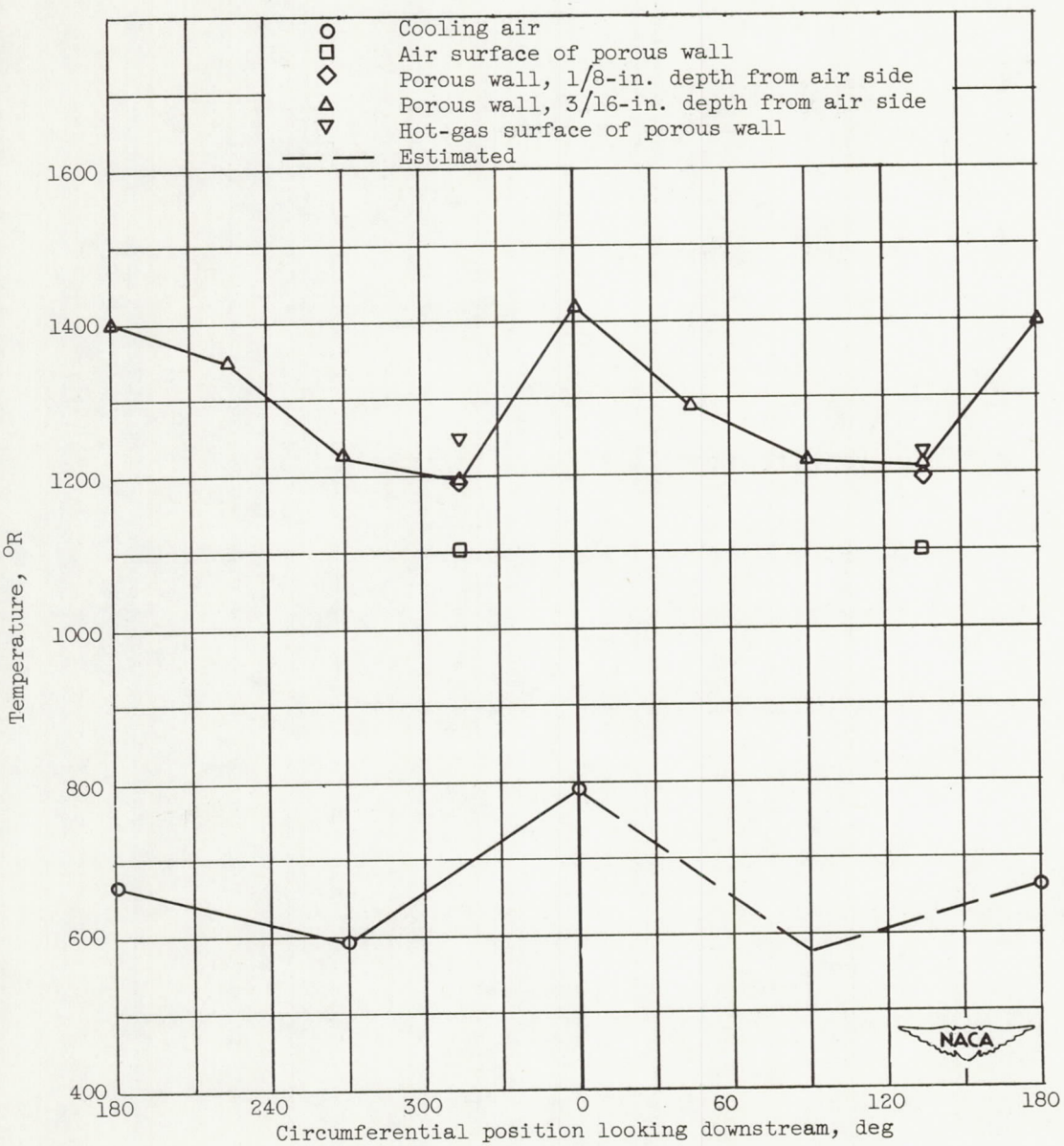

(a) Station A.

Figure 9. - Typical circumferential temperature profiles. Exhaust-gas total temperature, 3057° R; burner-inlet total temperature, 1579° R; inlet cooling-air temperature, 550° R; coolant-flow ratio, 0.093.

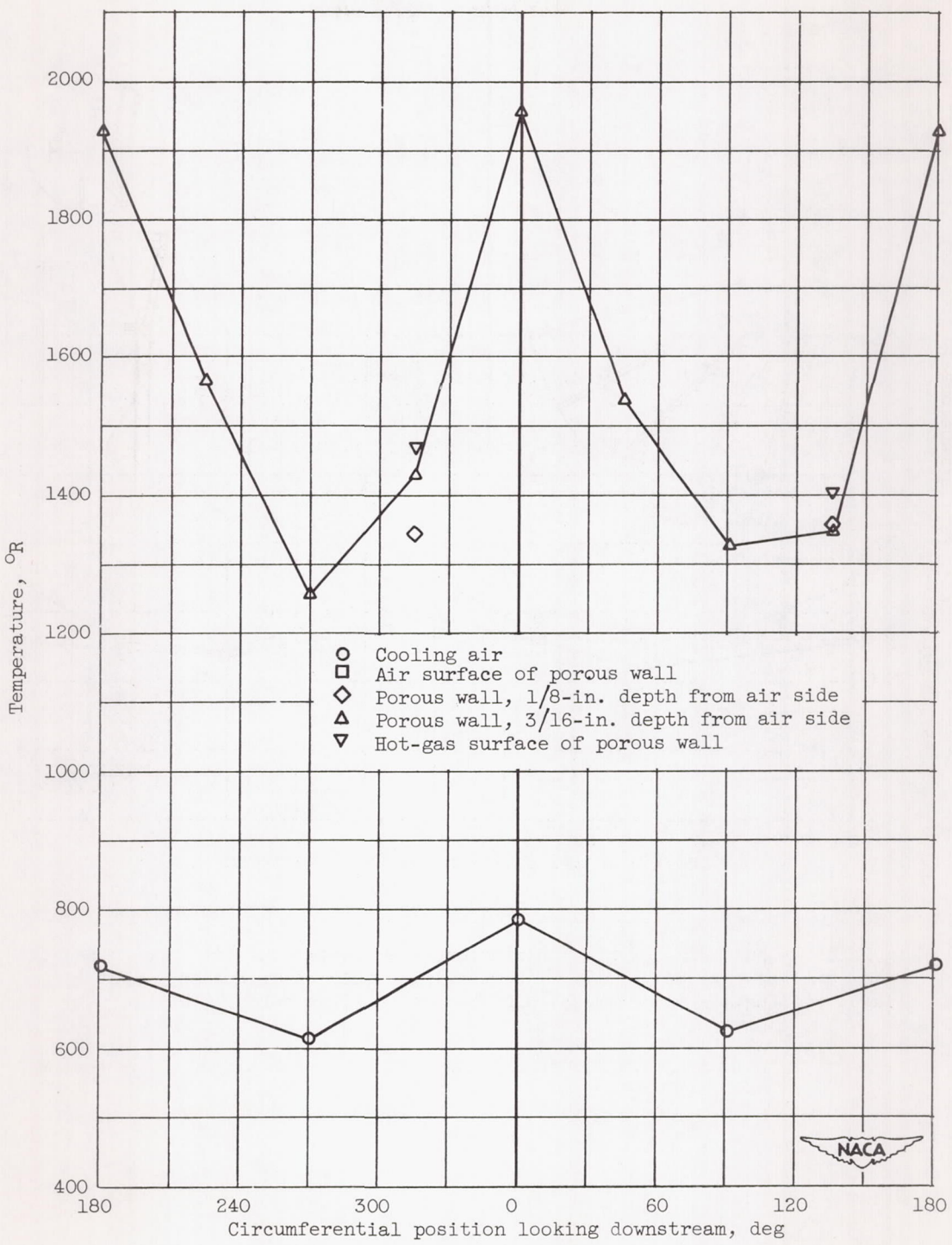

(b) Station B.

Figure 9. - Continued. Typical circumferential temperature profiles. Exhaust-gas total temperature, 3057° R; burner-inlet total temperature, 1579° R; inlet cooling-air temperature, 550° R; coolant-flow ratio, 0.093.

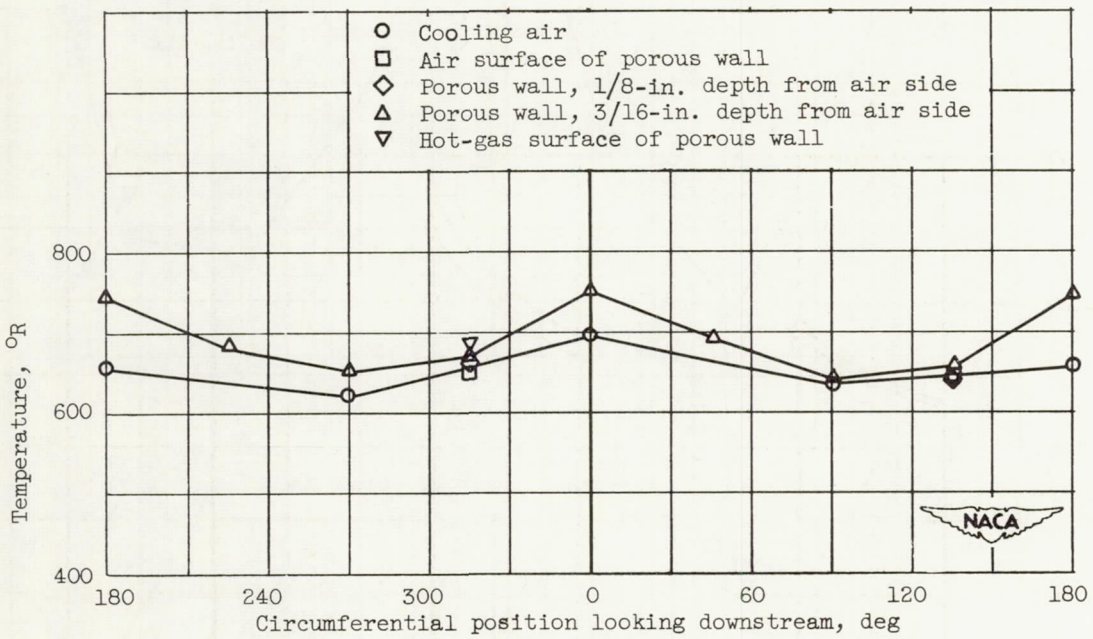

(c) Station C.

Figure 9. - Concluded. Typical circumferential temperature profiles. Exhaust-gas total temperature, 3057° R; burner-inlet total temperature, 1579° R; inlet cooling-air temperature, 550° R; coolant-flow ratio, 0.093.

CF-5 back

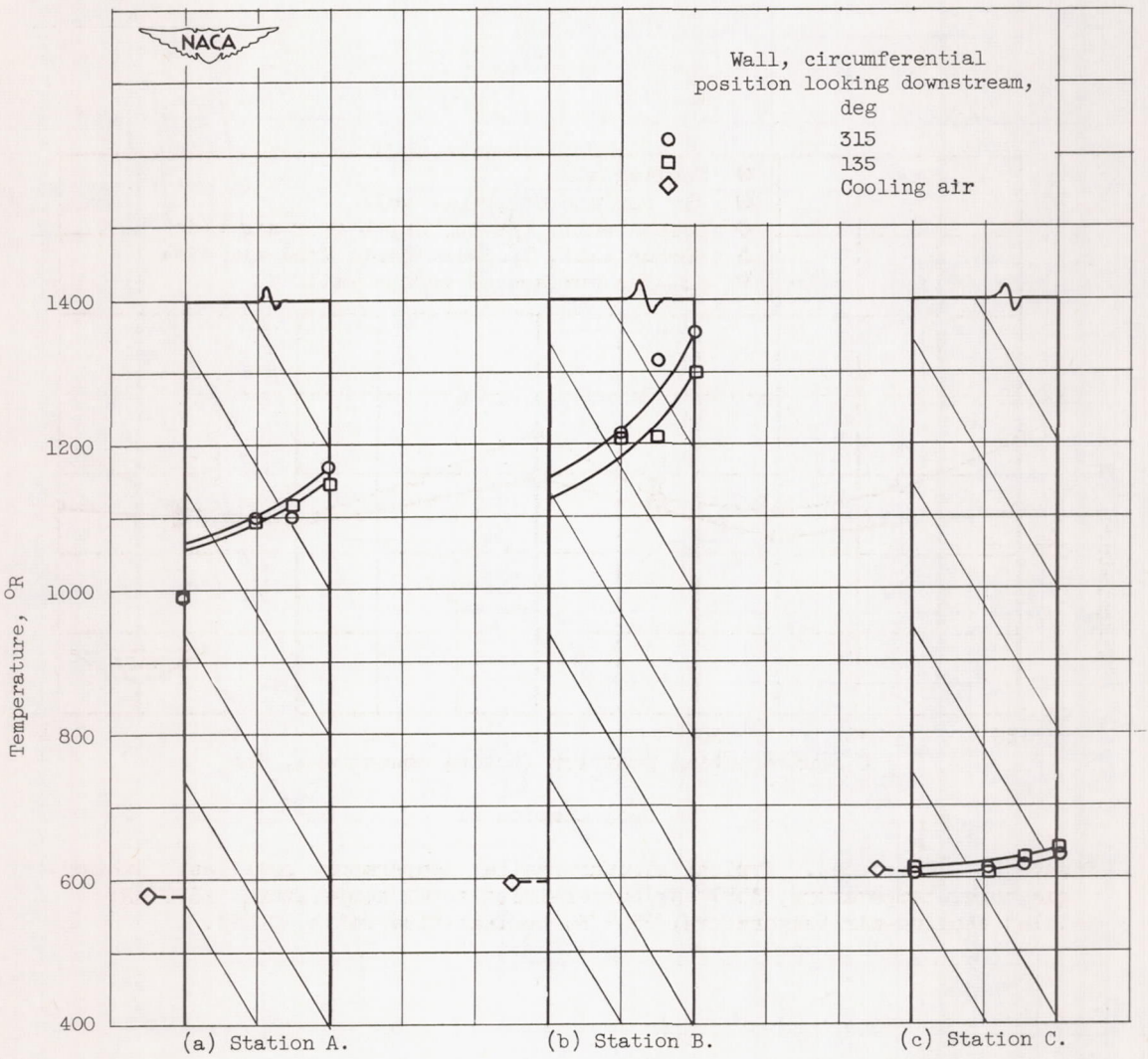

Figure 10. - Typical transverse temperature profiles for porous wall.

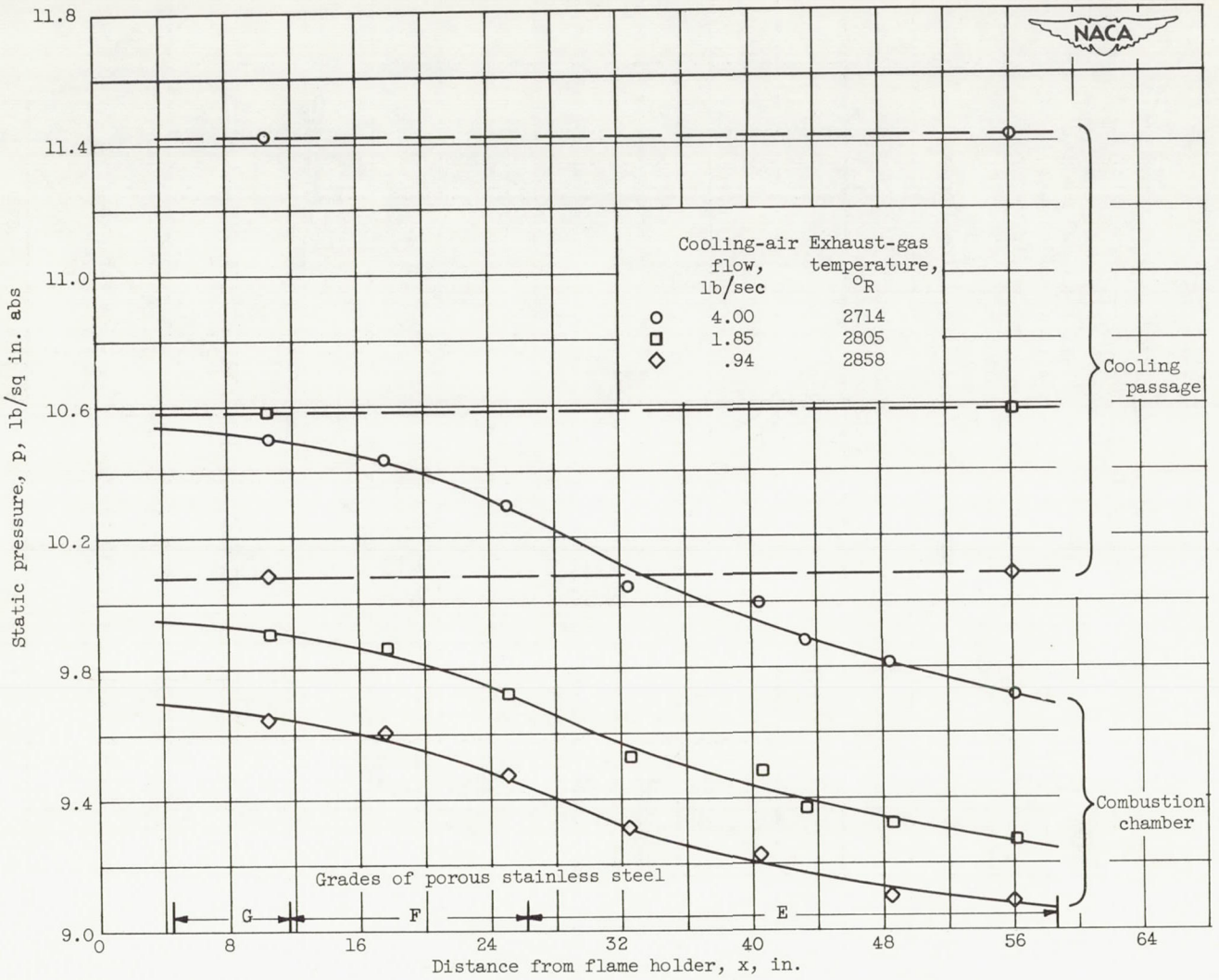

Figure 11. - Typical longitudinal static-pressure gradients in the cooling-air passage and in the combustion chamber.

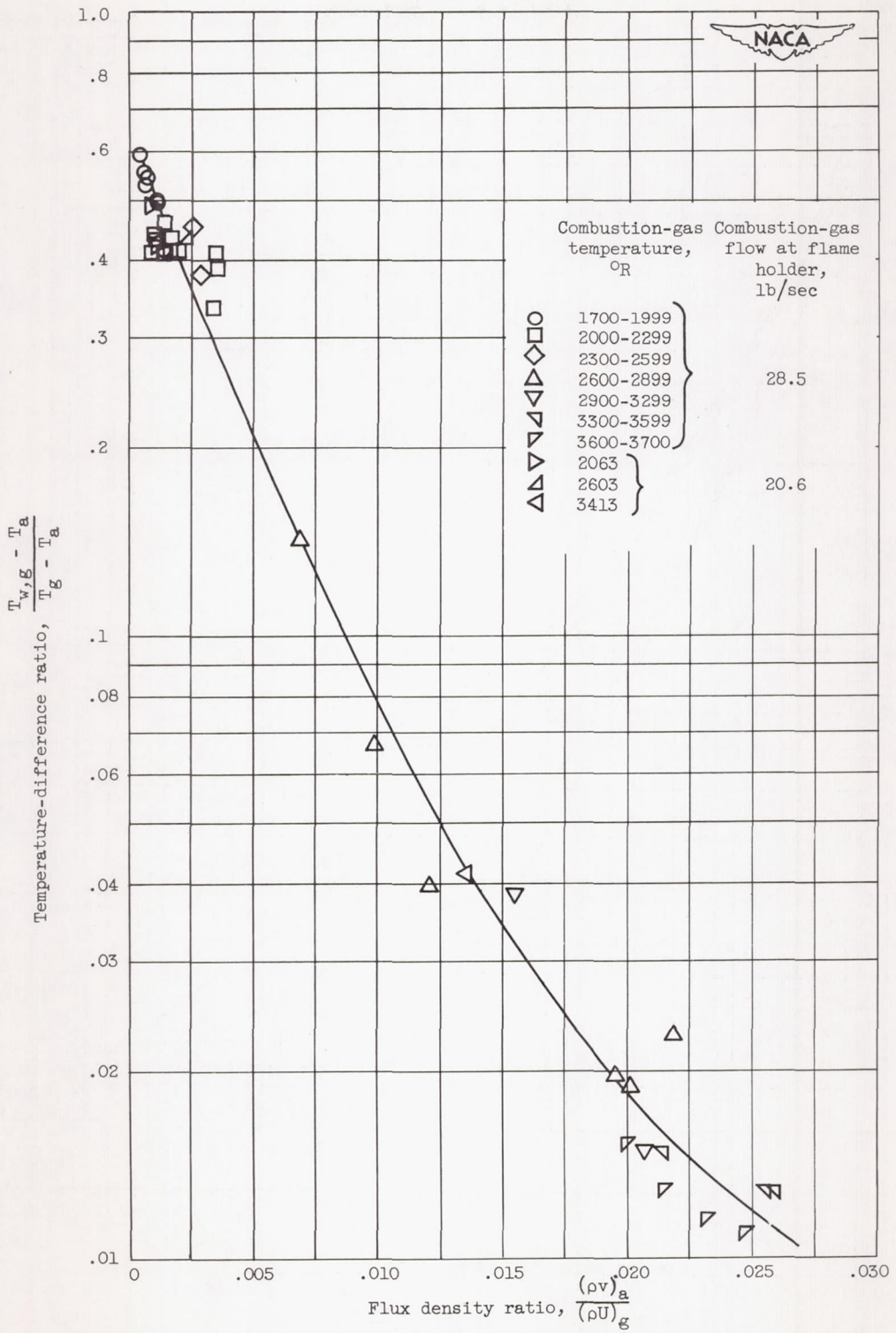

Figure 12. - Correlation of cooling data from experimental afterburner cooled by transpiration of air through sintered, porous stainless steel.

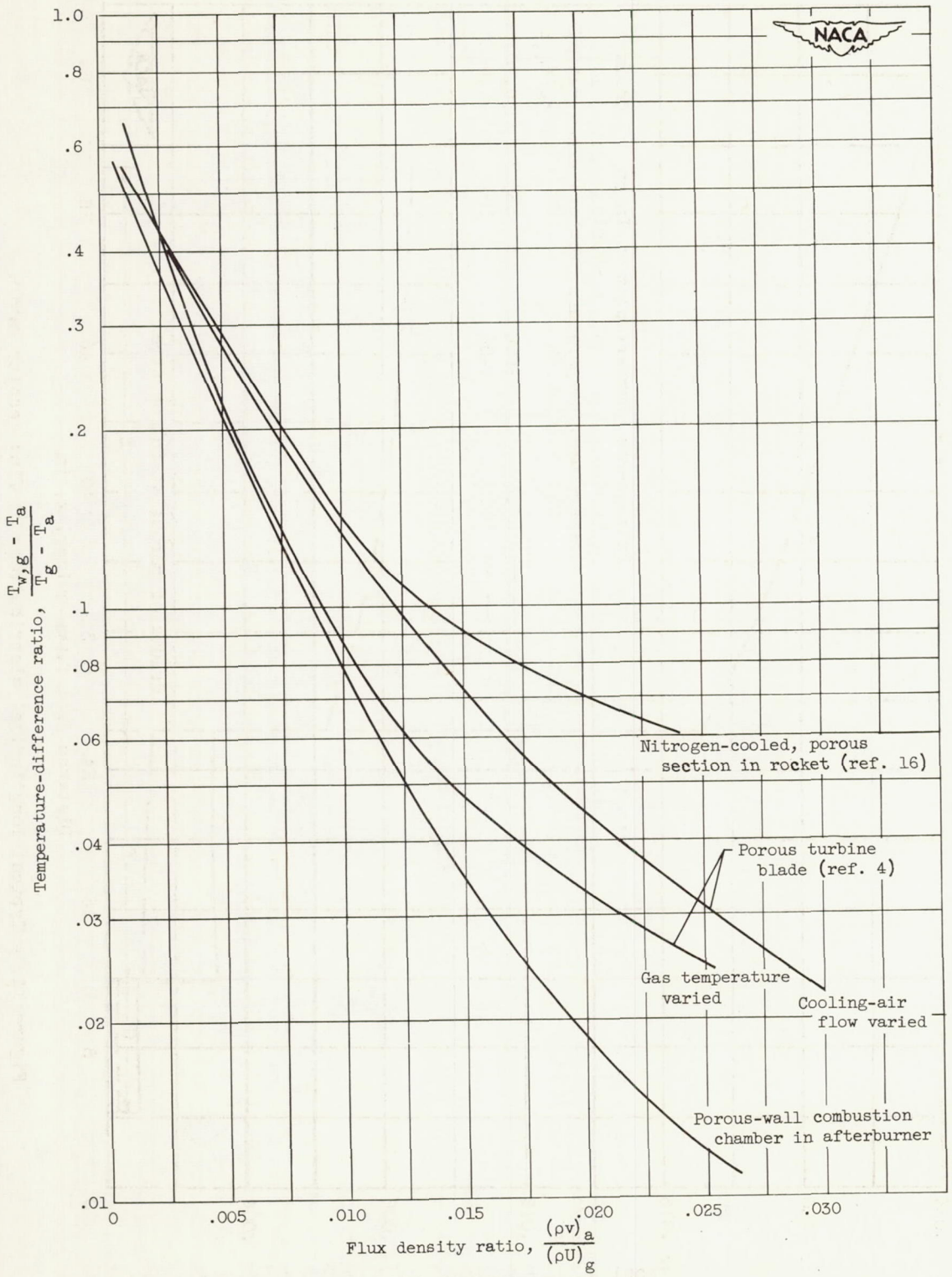

Figure 13. - Comparison of experimental cooling correlations for transpiration-cooled afterburner combustion chamber, turbine blade, and rocket.

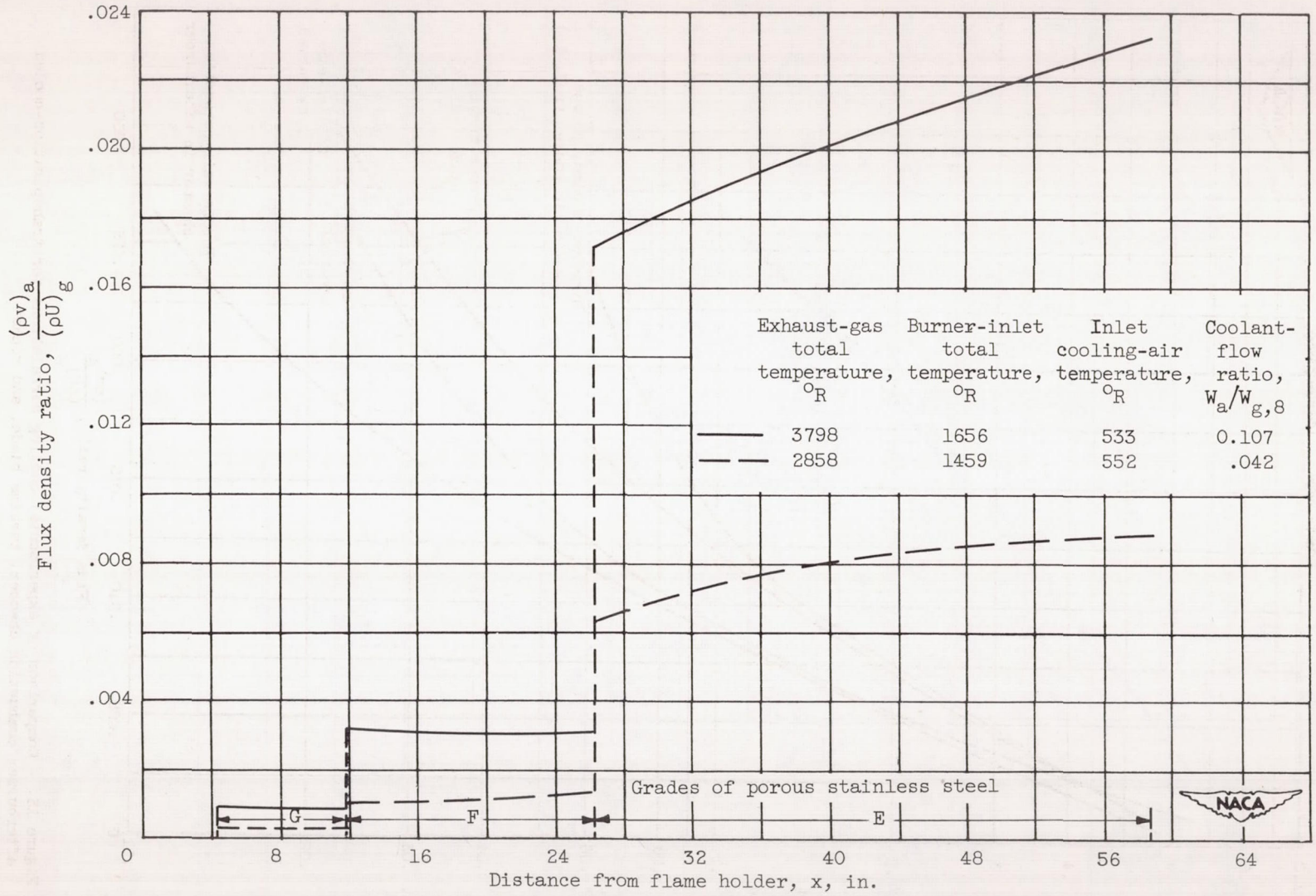

Figure 14. - Typical longitudinal distributions of flux density ratio.

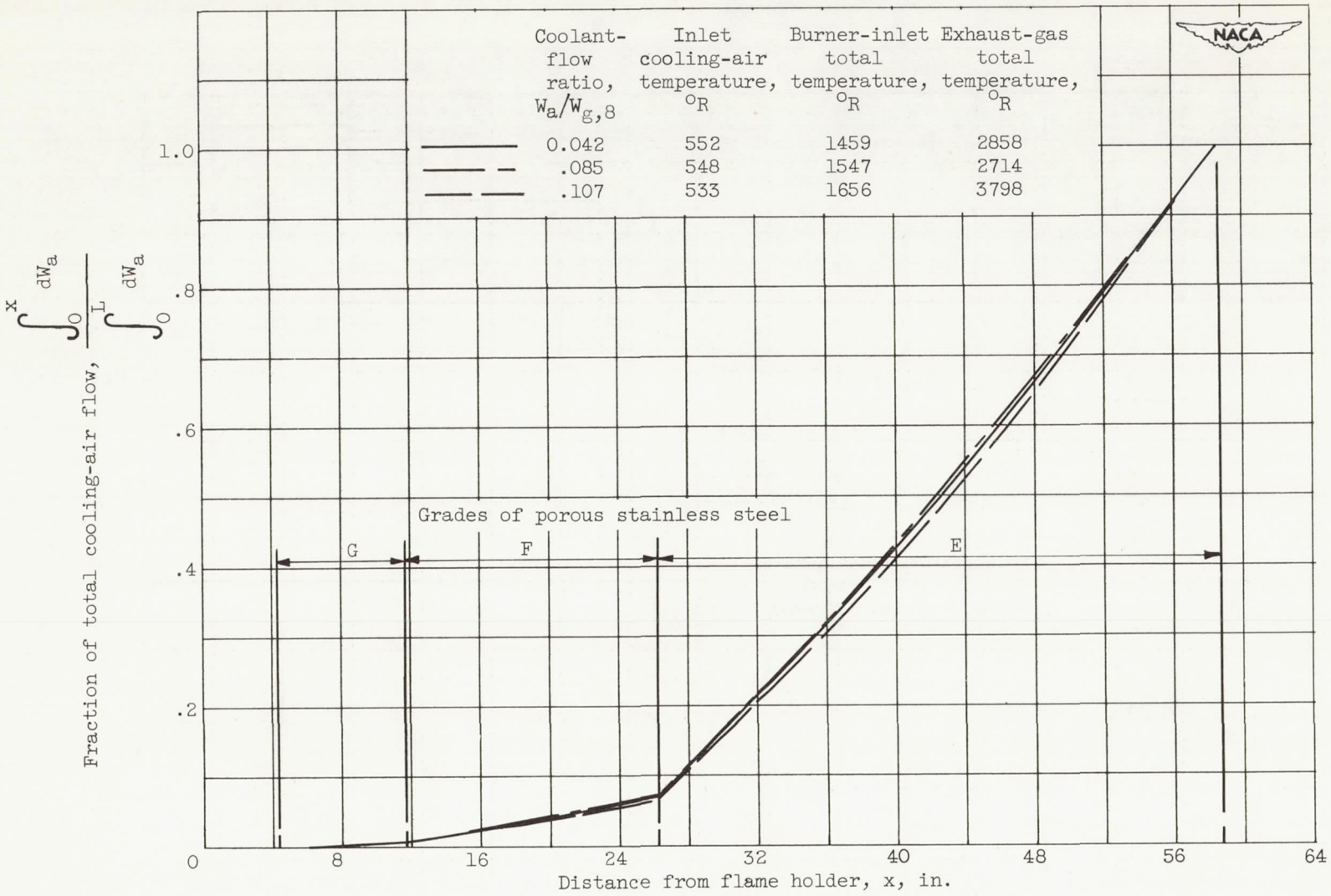

Figure 15. - Typical longitudinal distributions of cooling-air flow in experimental afterburner.

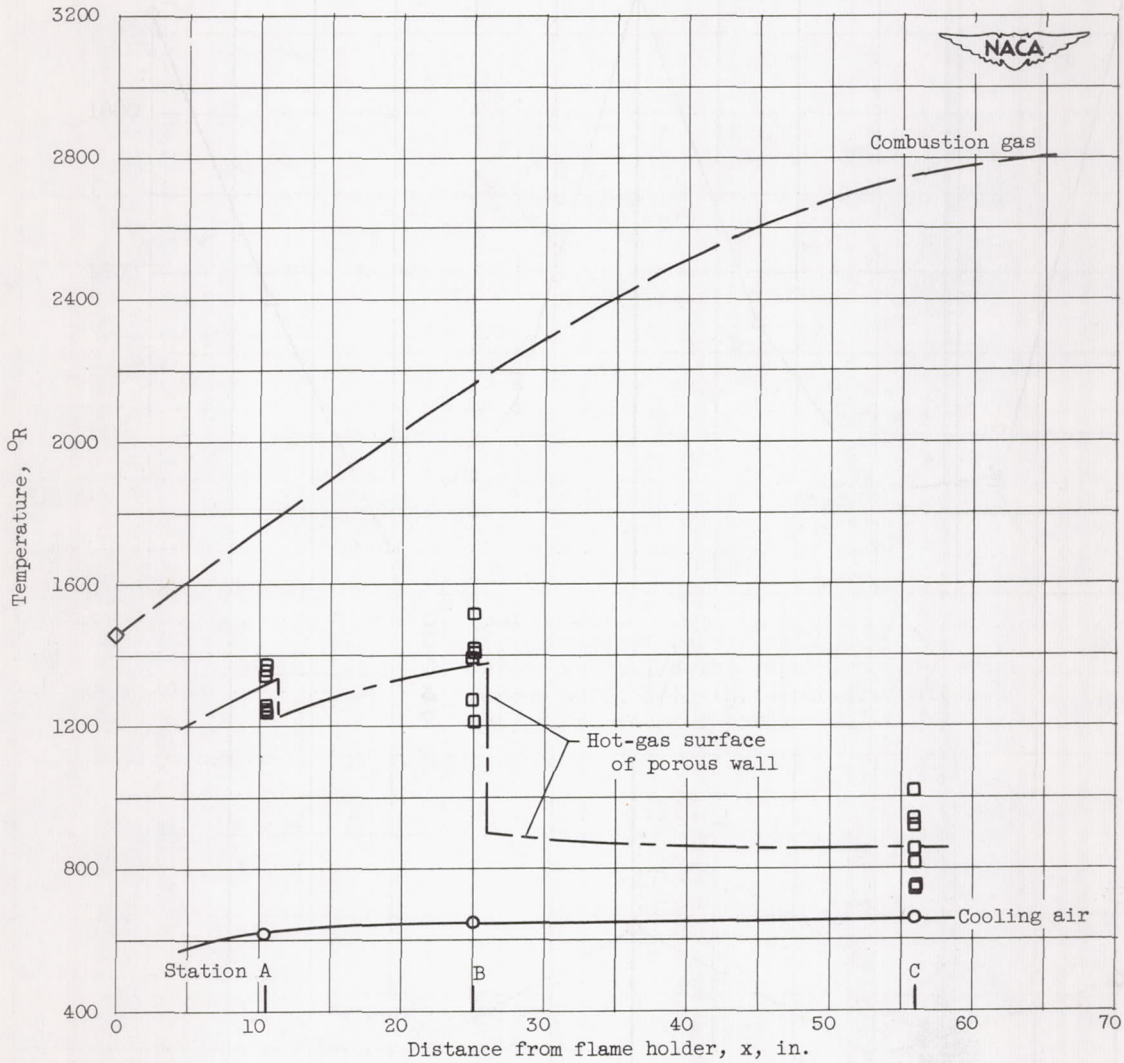

(a) Exhaust-gas total temperature, 2858° R; burner-inlet total temperature, 1459° R; inlet cooling-air temperature, 552° R; coolant-flow ratio, 0.042; cooling-air pressure, 10.09 pounds per square inch absolute; pressure drop across porous wall, 0.41 pounds per square inch at upstream end, 1.02 pounds per square inch at downstream end; total gas flow at exhaust-nozzle exit, 29.47 pounds per second.

Figure 16. - Longitudinal distribution of temperatures.

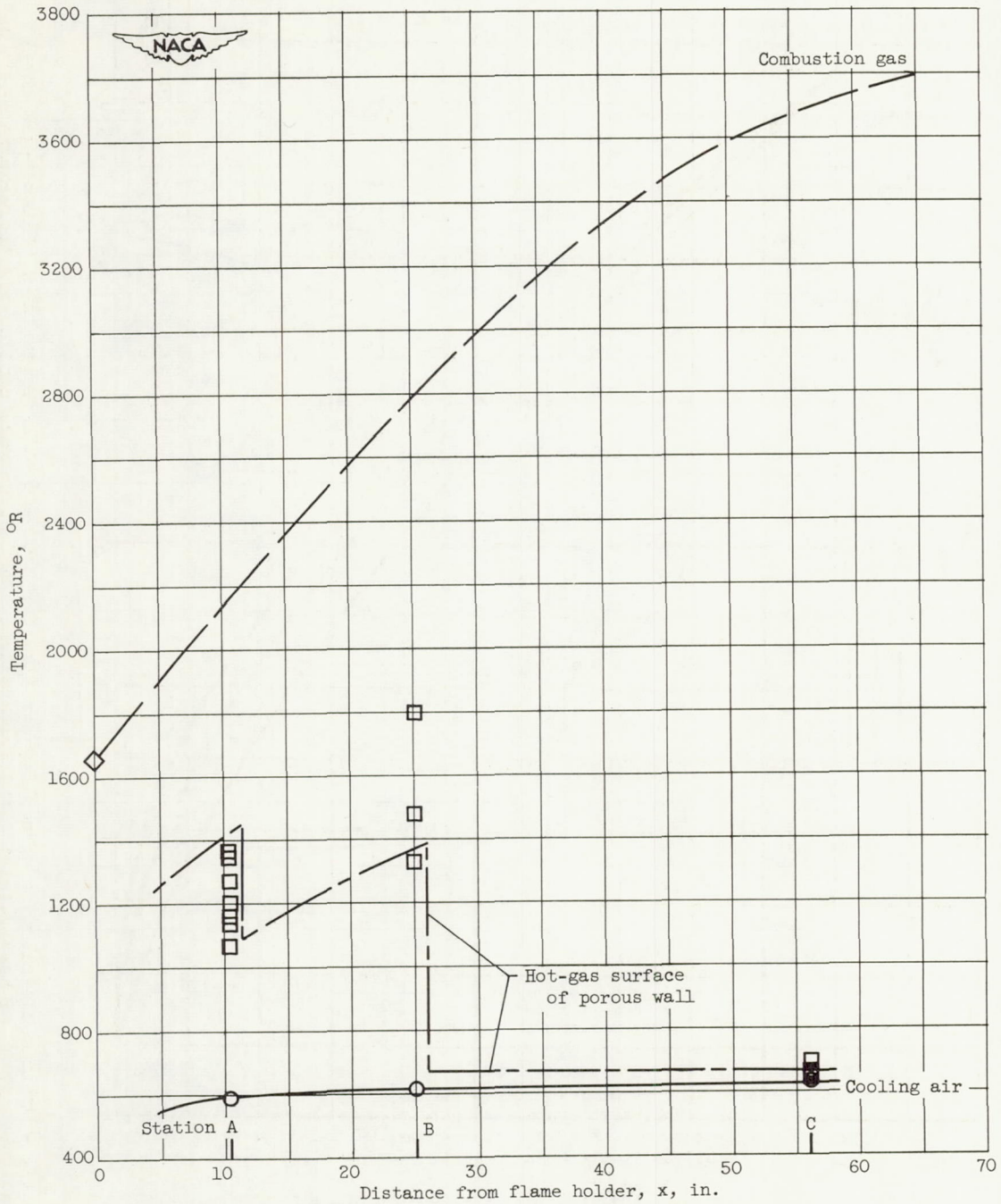

(b) Exhaust-gas total temperature, 3798° R; burner-inlet total temperature, 1656° R; inlet cooling-air temperature, 533° R; coolant-flow ratio, 0.107; cooling-air pressure, 12.36 pounds per square inch absolute; pressure drop across porous wall; 0.95 pounds per square inch at upstream end, 2.32 pounds per square inch at downstream end; total gas flow at exhaust-nozzle exit, 32.57 pounds per second.

Figure 16. - Concluded. Longitudinal distribution of temperatures.

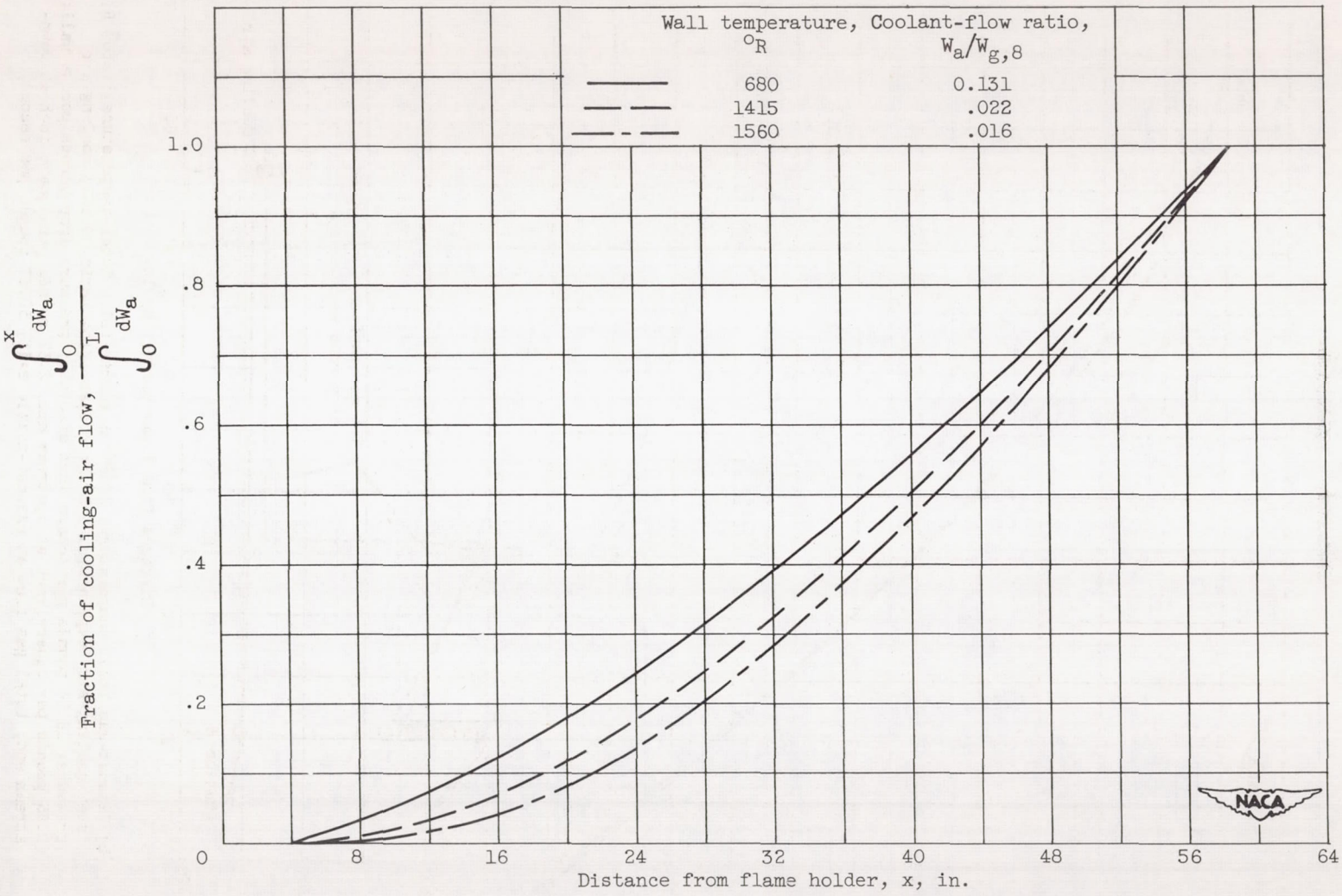

Figure 17. - Optimum distribution of cooling-air flow for constant wall temperature. Exhaust-gas total temperature, 3798° R; burner-inlet total temperature, 1656° R; average cooling-air temperature, 620° R; combustion-gas flow at flame holder, 29.1 pounds per second.

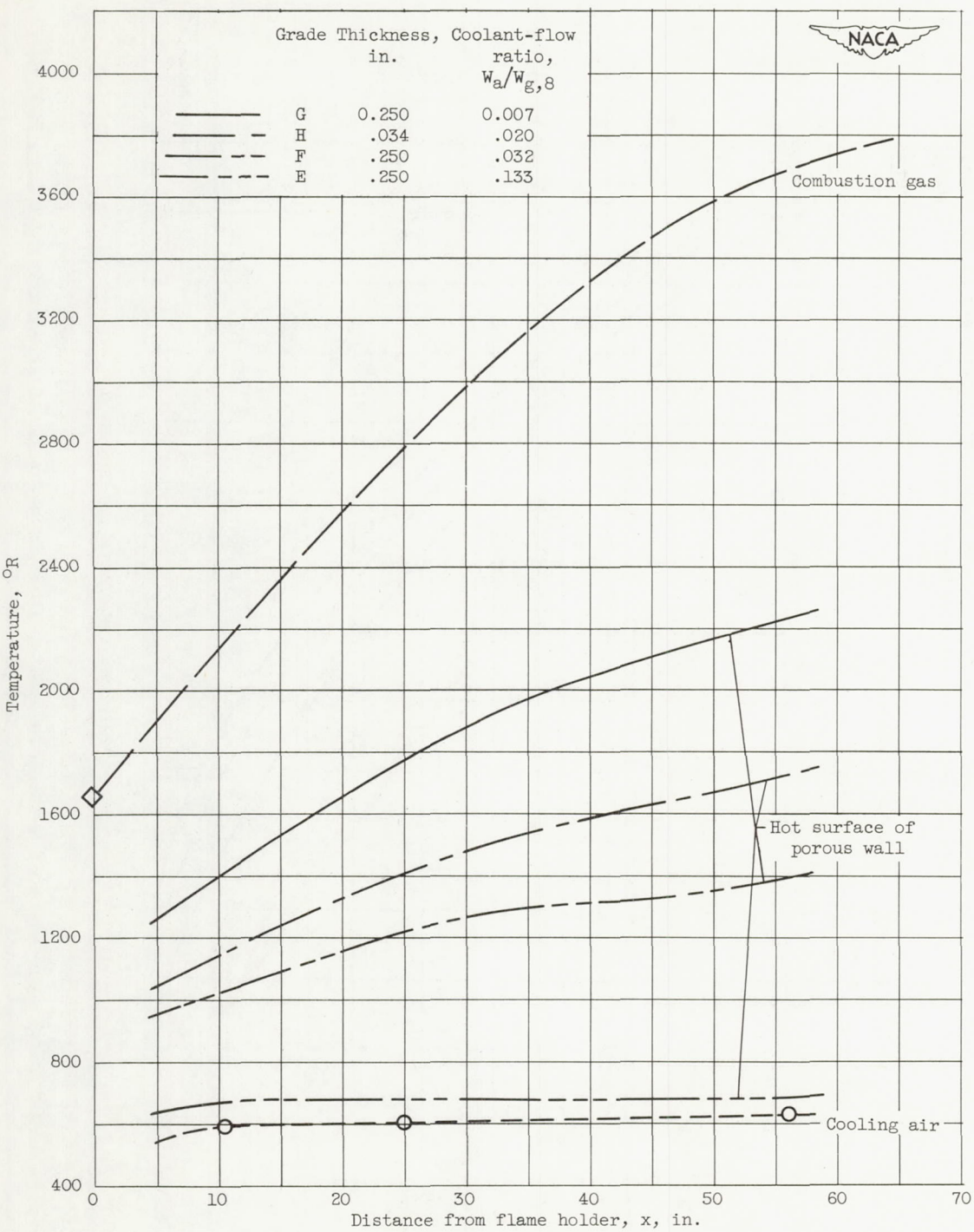

(a) Temperature distributions.

Figure 18. - Longitudinal distributions of temperature and cooling air for several uniform-permeability porous-wall combustion chambers. Exhaust-gas total temperature, 3798° R; burner-inlet total temperature, 1656° R; inlet cooling-air temperature, 533° R; cooling-air static pressure, 12.36 pounds per square inch absolute; combustion-gas flow at flame holder, 29.1 pounds per second.

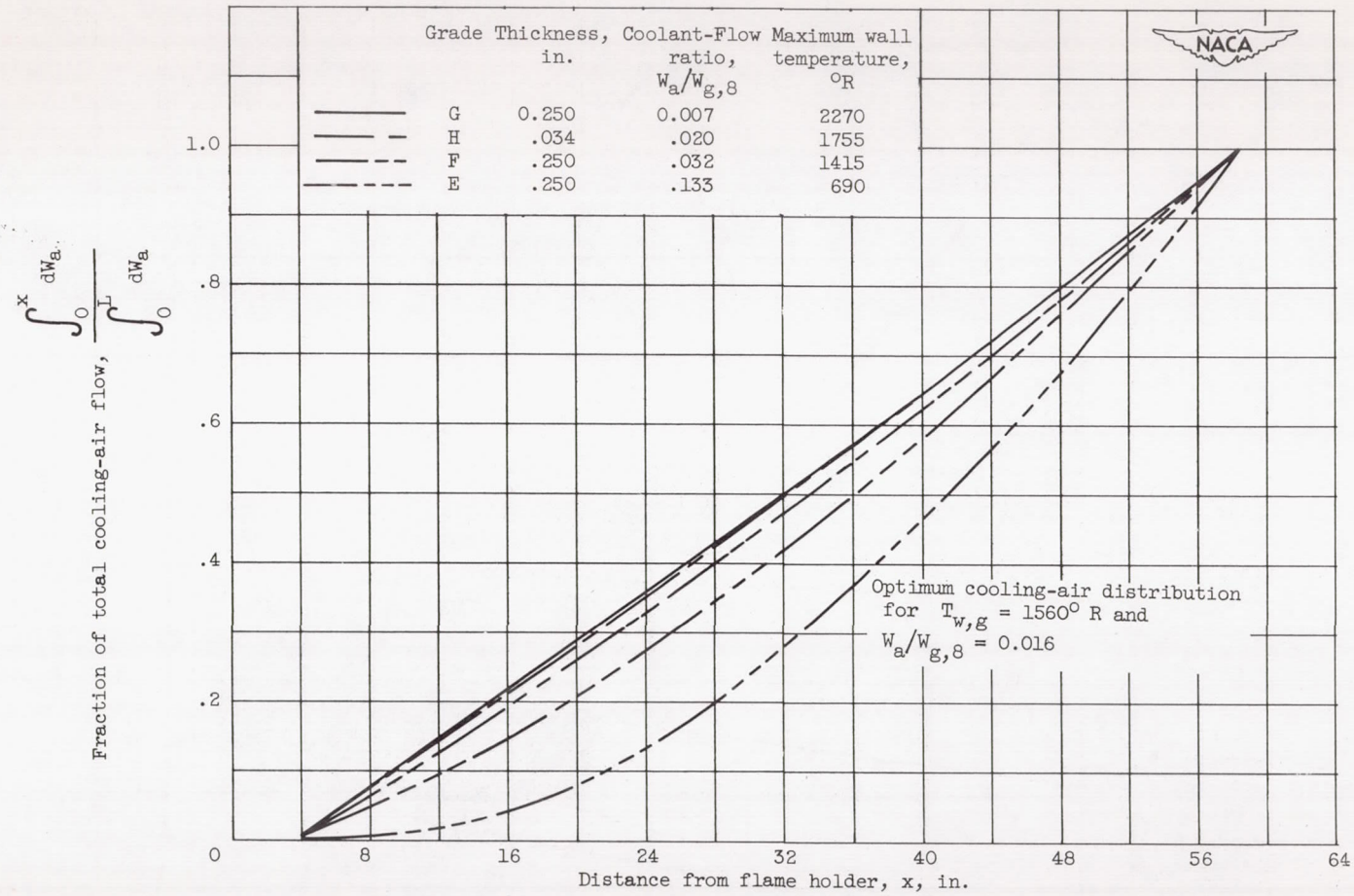

(b) Cooling-air distributions.

Figure 18. - Concluded. Longitudinal distributions of temperature and cooling air for several uniform-permeability porous-wall combustion chambers. Exhaust-gas total temperature, 3798° R; burner-inlet total temperature, 1656° R; inlet cooling-air temperature, 533° R; cooling-air static pressure, 12.36 pounds per square inch absolute; combustion-gas flow at flame holder, 29.1 pounds per second.

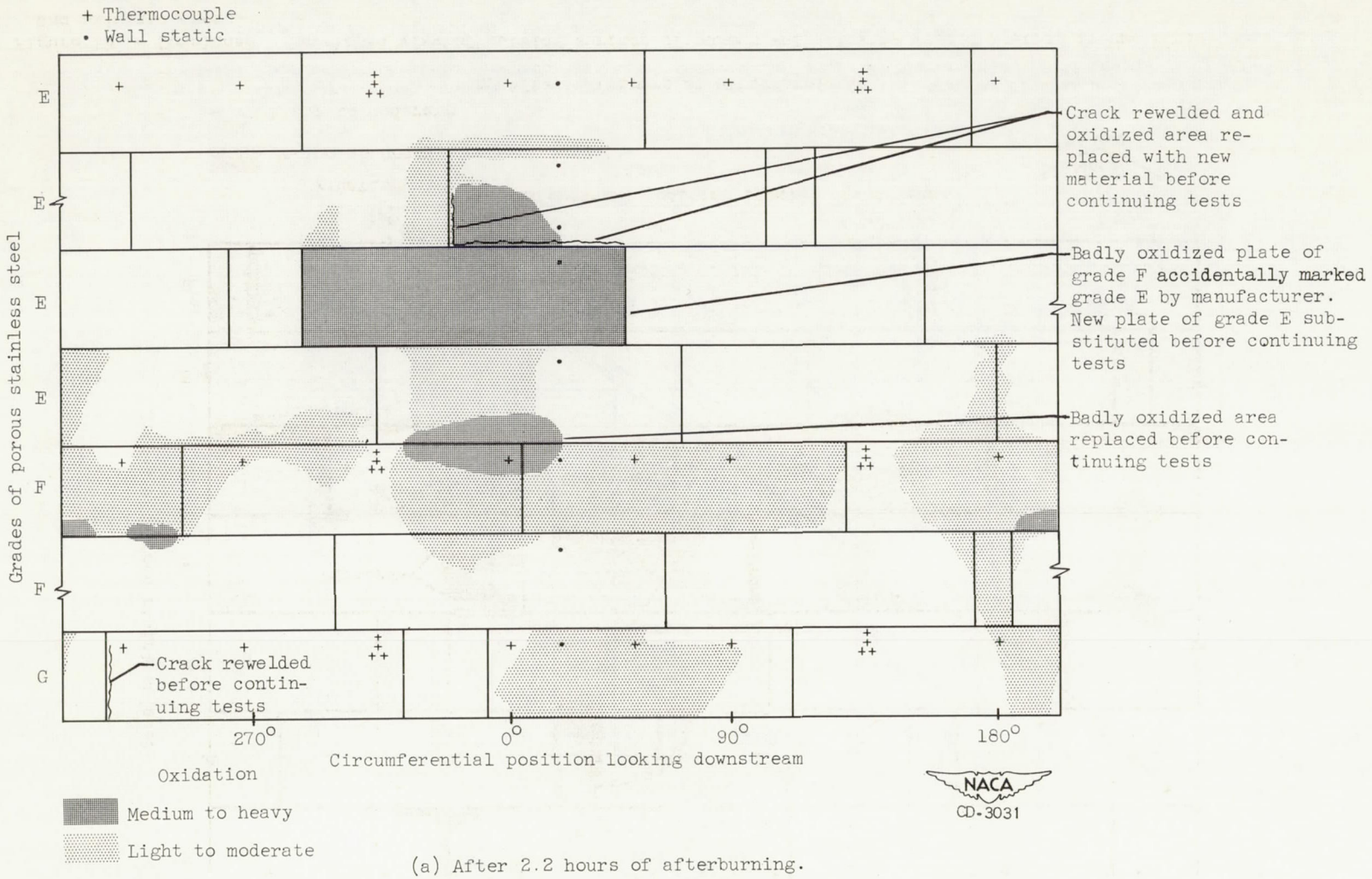

(a) After 2.2 hours of afterburning.

Figure 19. - Developed view of outside surface of porous wall showing welded plates, thermocouple locations, and oxidized areas.

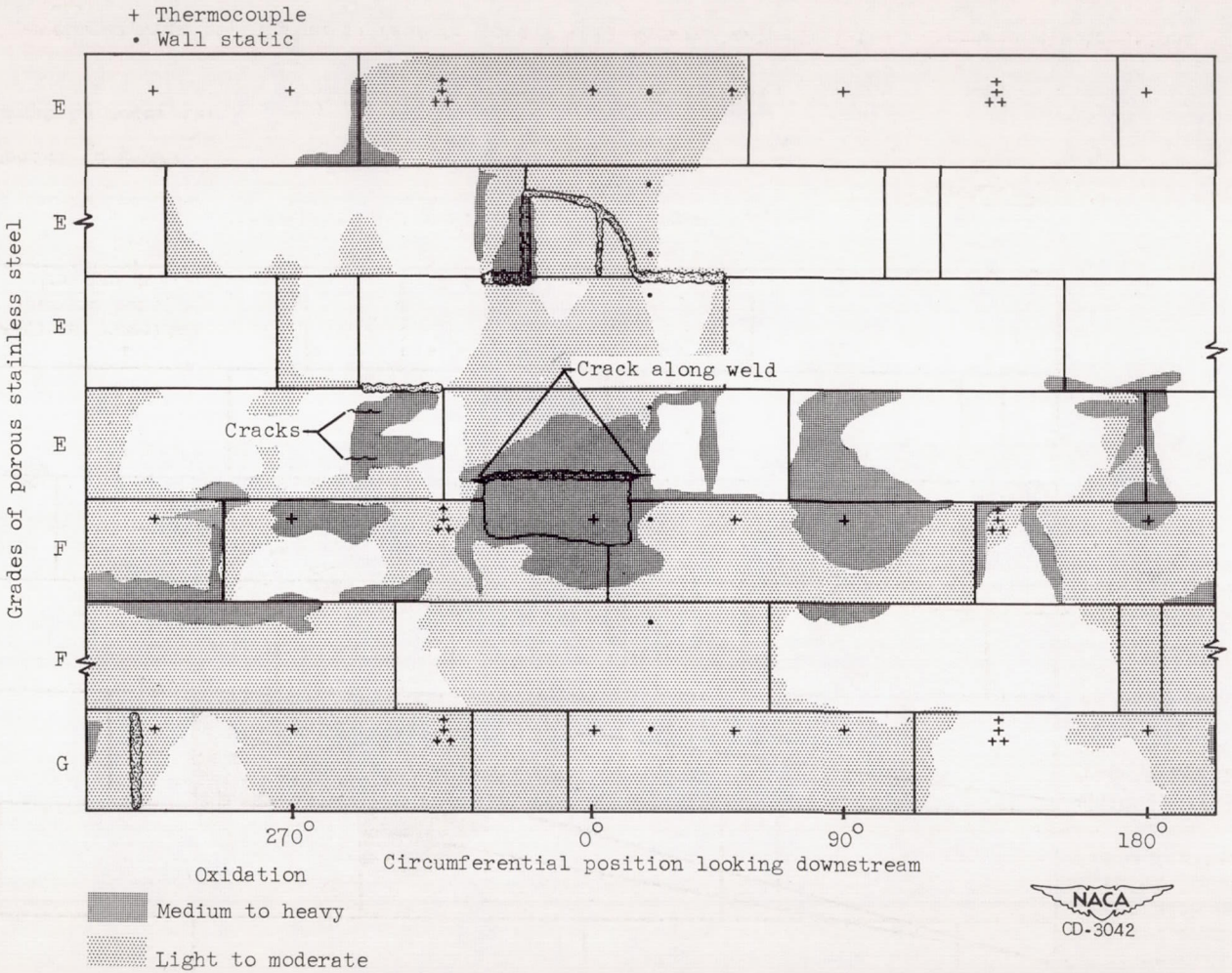

(b) After 6.2 hours of afterburning.

Figure 19 - Concluded. Developed view of outside surface of porous wall showing welded plates, thermocouple locations, and oxidized areas.